JGR Earth Surface

RESEARCH ARTICLE
10.1029/2022JF006666

Can Lava Flow Like Water? Assessing Applications of Critical Flow Theory to Channelized Basaltic Lava Flows

H. R. Dietterich[1], G. E. Grant[2], B. Fasth[3], J. J. Major[4], and K. V. Cashman[5]

[1]USGS Alaska Volcano Observatory, Anchorage, AK, USA, [2]U.S. Forest Service, Pacific Northwest Research Station, Corvallis, OR, USA, [3]College of Earth, Ocean, and Atmospheric Sciences, Oregon State University, Corvallis, OR, USA, [4]USGS Cascades Volcano Observatory, Vancouver, WA, USA, [5]Department of Earth Sciences, University of Oregon, Eugene, OR, USA

Key Points:

- Undular hydraulic jumps, or standing wave trains, form in both water and active lava at critical flow (Froude number ~1)
- Wavelengths scale with flow depth and velocity following hydraulic theory in water flume experiments and Hawaiian lava flow data
- Application to wave trains in active lava flows provides rapid estimates of key flow parameters and effusion rates for hazard assessment

Supporting Information:

Supporting Information may be found in the online version of this article.

Correspondence to:

H. R. Dietterich,
hdietterich@usgs.gov

Citation:

Dietterich, H. R., Grant, G. E., Fasth, B., Major, J. J., & Cashman, K. V. (2022). Can lava flow like water? Assessing applications of critical flow theory to channelized basaltic lava flows. *Journal of Geophysical Research: Earth Surface*, *127*, e2022JF006666. https://doi.org/10.1029/2022JF006666

Received 7 MAR 2022
Accepted 13 AUG 2022

Author Contributions:

Conceptualization: H. R. Dietterich, G. E. Grant, J. J. Major, K. V. Cashman
Data curation: H. R. Dietterich, B. Fasth
Formal analysis: H. R. Dietterich, G. E. Grant, B. Fasth, K. V. Cashman
Investigation: H. R. Dietterich, G. E. Grant, B. Fasth, J. J. Major, K. V. Cashman
Methodology: H. R. Dietterich, J. J. Major
Validation: H. R. Dietterich, B. Fasth
Visualization: H. R. Dietterich, B. Fasth
Writing – original draft: H. R. Dietterich, G. E. Grant, B. Fasth, J. J. Major, K. V. Cashman

Abstract Flowing lava and water have dramatically different physical properties but can form similar hydraulic structures, including undular hydraulic jumps, or standing wave trains. In water flows, undular hydraulic jumps are evidence of critical flow (Froude number ~1) and open-channel hydraulic theory provides a powerful tool for estimating flow depth and velocity. Monitoring these parameters in an active lava channel is inherently challenging, but essential for calculating lava discharge (effusion rate), a primary control on the rate of flow front advance and ultimate flow runout distance. We analyze undular hydraulic jumps in both water and lava flows to assess the conditions under which they form and, by extension, the potential use of critical flow theory to estimate, in real time, lava flow velocity, depth, and discharge. Experimental data for water flows show that these structures mark the transition from supercritical to subcritical flow. Undular hydraulic jumps in the near-vent lava channel of the 2018 lower East Rift Zone eruption of Kīlauea, Hawai'i also reflect critical flow conditions; their wavelengths scale with flow depth and velocity, consistent with hydraulic theory. Calculated lava effusion rates are similar to estimates made using more traditional approaches (Jeffreys', 1925, https://doi.org/10.1080/14786442508634662, equation based on lava viscosity, density, and channel slope) and with lava volumes derived from topographic-change mapping. From this we conclude that critical flow phenomena show great potential to track flow dynamics and inform hazard assessment for a wide range of geophysical fluids.

Plain Language Summary Flowing water and lava have very different physical properties, but under certain flow conditions, each will form arrays of evenly spaced standing waves (wave trains). In water, these are known to form at "critical flow" when there is a specific ratio between flow depth and flow velocity. However, conditions for forming standing wave trains in lava have not been measured. We investigated the relationship between the spacing of waves in a train, and the flow speed and depth, using both data from experiments with water and measurements made during the 2018 lava flow at Kīlauea volcano. We found that waves form in each fluid at the same ratio of flow speed and depth, and that the spacing of waves in a train shows a fixed mathematical relationship to these parameters. There is considerable practical importance to this finding. During a volcanic eruption, direct measurement of flow speed is difficult and dangerous, and depth is impossible, and yet both are needed to predict how far and how fast lava will travel. The critical flow characteristics of lava, and potentially other hazardous flows such as mudflows, allow assessment of flow behavior and potential hazards in real time.

1. Introduction

The two great geophysical liquids present at Earth's surface—water and molten lava—share common features. Despite orders of magnitude differences in viscosity and temperature (water = 8.9×10^{-4} Pa s at 25°C; basaltic lava = 50 Pa s at 1200°C), both liquids form gravity currents that, under the right circumstances, exhibit flow features such as turbulence, eddies, standing waves, and hydraulic jumps. In water flows, the full complement of these features occurs in channels with steep slopes (S) > 0.01 m/m (~0.6°), such as those in mountain or canyon rivers, where flow velocities reach 1–10 m/s and complex flow features manifest as whitewater rapids. These features are often triggered by external influences, such as step changes in channel-bed elevation or channel width, substantive changes in slope, large boulders, or other conditions that cause abrupt changes in flow velocity. The circumstances that promote these same flow features in lava are not well constrained but observations show that they are most common close to volcanic vents where lava temperatures and flow velocities are high,

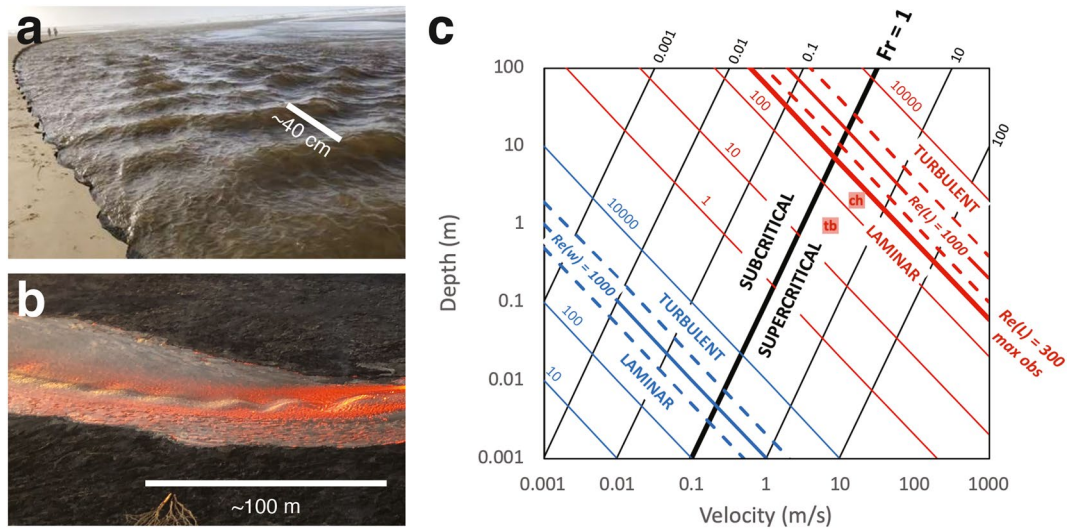

Figure 1. (a) Oblique photograph of undular hydraulic jumps in a water channel on the Oregon Coast (credit: Gordon Grant). (b) Oblique USGS/HVO photograph of undular hydraulic jumps in a lava channel on 13 June 2018, during the 2018 eruption of Kīlauea, HI (credit: Bruce Houghton). (c) Log-log plot of flow velocity versus flow depth, contoured for Froude (Fr) number (black lines) and Reynolds (Re) number (blue lines show Re for water, red lines show Re for lava). Near-vent values for vesicular lava of $\rho = 1{,}000$ kg/m^3 and $\mu = 200$ Pa s are assumed. For water, $\rho = 1{,}000$ kg/m^3 and $\mu = 0.001$ Pa s are assumed. Red boxes labeled ch (channel) and tb (tube) show maximum flow conditions reported for observed standing waves in lava flows (Dietterich et al., 2021; Kauahikaua et al., 1998; Lipman & Banks, 1987).

viscosities are low, and solidification is minimal. In large part, this lack of constraints reflects the paucity of direct observations of lava flows in space and time. Until recently, even well documented eruptions have been monitored intermittently only at discrete points along the flow, and often only in the more easily accessible medial to distal channel locations.

Here, we take advantage of a unique set of observations collected along a single channelized lava flow during the 2018 eruption of Kīlauea volcano, Hawai'i, USA. We focus on a particular flow feature—undular hydraulic jumps—that manifest as a train of standing waves. Undular hydraulic jumps are observed in water (Chanson, 1995; Fawer, 1937; Gilbert, 1914; Grant, 1997; Henderson, 1966; Kennedy, 1961, 1963; Kieffer, 1985; Murphy, 1910; Ohtsu et al., 2003; Tinkler, 1997), lahars (Cronin et al., 1999; Gudmundsson, 2015; Pierson, 1985; Pierson & Scott, 1985; Pringle & Cameron, 1999; Rodolfo et al., 1996) and, as we demonstrate here, lava flows (Figures 1a and 1b). In contrast to other types of standing waves, including single hydraulic jumps and lateral shock waves (which are commonly located at abrupt slope or width transitions), undular hydraulic jumps do not require slope or width transitions to form; importantly, they represent a distinctive train of standing waves that can be used to infer flow conditions. In this paper we focus exclusively on undular hydraulic jumps, which differ from other types of standing waves in their hydraulic properties and architecture. Observations of analogous wave patterns in lava are largely anecdotal and have been reported most commonly for fast-moving Hawaiian lava flows (e.g., Dietterich et al., 2021; Finch & Macdonald, 1953; Kauahikaua et al., 1998; Macdonald, 1943; Wolfe, 1988), although they have also been described in low viscosity lava flows from La Palma (Castro & Feisel, 2022). A recent paper by Le Moigne et al. (2020) suggested that open-channel hydraulic theory for hydraulic jumps, particularly those formed by changes in flow geometry, can be applied to lava flows to infer both flow dynamics and key physical properties. However, the hypothesis that similar flow features in water and lava reveal similarities in their underlying physics and hydraulics needs greater scrutiny. Specifically, a clear mechanistic understanding of flow conditions giving rise to different types of standing waves in both water and lava is required, as is testing of underlying theory and assumptions using detailed field measurements.

Understanding the physical circumstances that produce undular hydraulic jumps in lava flows is of more than academic interest. Fast-moving lava flows pose hazards to lives, homes, and infrastructure. For this reason, models that forecast rates and routes of lava-flow advance can help to anticipate this hazard, but only if erup-

tion rates at the vent are well constrained (see Harris et al., 2007, 2016). With better sensors, satellite-based estimates of effusion rates have improved (Carn, 2016; Coppola et al., 2016), although these remote observations provide only time-averaged minimum effusion rates (Garel et al., 2016; Harris & Baloga, 2009). Real-time observations of vent activity have also improved, particularly with the opportunities provided by UAS (unoccupied aircraft systems) video, which can be used to determine the planform geometry of lava channels and the distribution of surface flow velocities. Accurate estimates of lava flux, however, require the third dimension, that is, flow depth. If analogies with river flows can be established, undular hydraulic jumps offer the potential for rapid assessment of not only lava flow depth, but also mean velocity, and, by extension, effusion rate.

The 2018 eruption of Kīlauea presented an exceptional opportunity to demonstrate the potential of applying undular hydraulic jump theory to lava-flow-hazard assessment. During this large and destructive eruption, undular hydraulic jumps were observed in the fast-moving, near-vent lava where flow velocities and channel widths were measured (Figure 1b). By assuming that hydraulics in lava and water flows are analogous, as suggested by preliminary work (Cashman et al., 2018), undular hydraulic jump theory was used to estimate lava flow depth and, by extension, effusion rates in near-real-time. An initial exploratory application of this method was promising, with good overall correspondence of calculated lava flow depths and effusion rates to independent measurements of depth, instantaneous effusion rate, and time-averaged discharge rate (Dietterich et al., 2021). The unprecedented detail of undular hydraulic jump documentation, including high-resolution lidar topographic data, UAS-based video, and field observations throughout the eruption, provides a unique data set to test initial assumptions and critically assess the extent to which analogous flow features in lava and water represent similar hydraulics.

Here, we examine fundamental mechanisms giving rise to undular hydraulic jumps in open-channel water flow by extracting key measurements of wave patterns and dynamics from published flume experiments to constrain their relations to velocity, depth, and discharge. We then apply these findings to quantitative observations from the 2018 eruption of Kīlauea to test critical assumptions and convergence with physical behavior of water. We use the results to calculate effusion rates, which are then compared against rates calculated by independent methods. Our results strongly suggest that fundamental hydraulic theory can be confidently applied to lava flows under the right circumstances to generate novel and rapid estimates of flow parameters and effusion rates.

2. Undular Hydraulic Jumps: Fundamental Hydraulics and Theory, Observations, and Flume Experiments in Water

2.1. Fundamental Physical Context for Shallow Flow of Water and Lava

Formal expressions for the conservation of mass, momentum, and energy describe the shallow flow of various fluids (e.g., Costa & Macedonio, 2005; Iverson & Denlinger, 2001; Vreugdenhil, 1994). For an incompressible, Newtonian viscous fluid, these expressions describe the balance of inertia, pressure, viscous, and gravity forces. From these expressions, groupings of dimensional parameters can be written in terms of two principal dimensionless numbers: Reynolds number (Re), which describes the ratio of inertia force to viscous force, and Froude number (Fr), which describes the ratio of inertia force to gravitational force. Assuming that near-vent lava flows can be treated, to first approximation, as isothermal Newtonian fluids (e.g., Takagi & Huppert, 2010), the influences of these key dimensionless numbers can be seen when the shallow-flow equations are written in dimensionless form. Under the conditions specified, the x-direction (longitudinal) component of the dimensionless, depth-averaged shallow-flow momentum equation takes the form of (e.g., Iverson & Denlinger, 2001; Vreugdenhil, 1994):

$$\frac{\partial u^* h^*}{\partial t^*} + \frac{\partial u^{*2} h^*}{\partial x^*} + \frac{\partial u^* v^* h^*}{\partial y^*} = \frac{h*}{Fr^2}\left[-\frac{\partial h^*}{\partial x^*} + 1\right] + \frac{1}{Re}\left[\frac{\partial^2 u^*}{\partial x^{*2}} + \frac{\partial^2 u^*}{\partial y^{*2}} - \frac{u^*}{h^*}\right] \quad (1)$$

in which starred parameters are dimensionless depth-averaged velocities (u*, v*), depth (h*), time (t*), and the longitudinal and spanwise spatial positions (x*, y*). Reynolds number and Froude number are written in terms of dynamic viscosity (μ), fluid density (ρ), gravitational acceleration (g), a reference velocity (u), and a reference length (L) as $Re = \rho u L/\mu$ and $Fr = u/\sqrt{gL}$. In shallow flows such as rivers and lava flows, the length scale (L) for both the Reynolds and Froude numbers is flow depth (d).

We provide this simplified and generalized single-direction component of the shallow-water equation solely to highlight key differences between flow regimes of water and lava flow. In high *Re* flows such as rivers (*Re* commonly 10^5–10^6), the viscous resistance term (far right-hand side) is negligible and flow is governed by a balance of inertia (left hand side) and pressure and gravity (combined first term right-hand side) forces. In contrast, *Re* in lava flows is orders of magnitude lower than for river flow (commonly ≤300) and viscous forces remain influential. Even so, lava flows can move at very high velocities (10–20 m/s) and, under those conditions, can have the unusual state of having low *Re* but high *Fr* (~1.5 to 5). When this occurs, lava flows have a fundamentally different physical behavior than water flow, as viscous forces continue to exert influence even in high velocity flows. A key question is whether this difference negates the applicability of fluvial open-channel hydraulics to lava flows? We maintain that under the proper assumptions, similar hydraulic theory can be reasonably applied to flows of both water and lava. In particular, we show that in both water and lava flows standing waves are characteristic of flows that are at or near critical flow (Henderson, 1966).

The distinction between low and high values of *Re* and *Fr* and consequent effects on flow behavior can be conceptualized in velocity-depth space, showing the boundaries between laminar and turbulent flow (defined by *Re*) and subcritical and supercritical flow (defined by *Fr*) (Figure 1c). In water flows, supercritical behavior typically occurs under turbulent flow conditions. In pipe flow, the transition from laminar to turbulent flow occurs at $500 \leq Re \leq 2{,}000$, although this transitional limit is for guidance only, as the transition from laminar to turbulent flow in open channels depends on local conditions (Sano & Tamai, 2016). Nevertheless, *Re* in river flows is commonly of order 10^6. In contrast, flow of lava at high velocities (>15 m/s) yields *Re* that are typically <300 (Figure 1c) owing to the high viscosity of lava ($\mu > 100$ Pa s) relative to that of water ($\mu \sim 0.001$ Pa s). This gives rise to the unusual condition of having low *Re* lava flows with high *Fr* that can indeed achieve supercritical flow conditions. Under these conditions lava flows exhibit either individual hydraulic jumps at abrupt topographic transitions, as observed in lava tubes (Kauahikaua et al., 1998), or undular hydraulic jumps in straight channel reaches. Moreover, although water and lava flows differ in terms of the relative importance of viscous forces, and hence the domains they occupy in Figure 1c, under high inertia conditions similar values of *Fr* can be achieved by both. The argument that hydraulic theory for water flow might be applied to lava flows under those conditions is bolstered by a long history of previous work using the shallow-water equations and fluvial hydraulics to model highly viscous natural flows, including snow avalanches (Eglit et al., 2020; Grigorian & Ostroumov, 2020) as well as eddies, shock waves and hydraulic jumps in granular and other highly dissipative flows (e.g., Amarouchene & Kellay, 2006; Boudet et al., 2007; Gray et al., 2003; Hákonardóttir & Hogg, 2005; Viroulet et al., 2017).

2.2. Theory of Undular Hydraulic Jumps From Studies of Water Flows

As previously noted, hydraulic jumps encompass a range of flow features, from individual stationary jumps to trains of stationary standing waves, termed undular hydraulic jumps. In river systems hydraulic jumps are common at the bases of dams, along engineered canals with abrupt changes in channel slope, below steps in bed topography, and where channel width changes abruptly. Hydraulic jumps form when the flow regime changes rapidly from supercritical to subcritical, which can be due to a change in river topography, or simply because of upstream supercritical flow encountering downstream subcritical flow. Our focus here is on undular hydraulic jumps, which are observed both in channels with deformable mobile beds (Kennedy, 1961, 1963) but also in fixed-bed channels (i.e., Chanson & Montes, 1995; Tinkler, 1997). Despite their common occurrence in varied settings, undular hydraulic jumps have received comparatively limited detailed study. Theoretical treatments of their occurrence in channels with deformable beds was developed by Kennedy (1961, 1963), who called them stationary waves, and current state of theory in fixed-bed channels is summarized by Castro-Orgaz and Chanson (2022). Extensive experimental work on undular hydraulic jumps has been done by Chanson and colleagues (Chanson, 1995, 2009; Montes & Chanson, 1998) and Ohtsu et al. (2001, 2003).

In water, undular hydraulic jumps are characterized as trains of undulating standing waves that typically diminish in amplitude with distance downstream and have distinctive architecture and dimensions (Figures 1a and 2, Table 1). Wave crests may or may not break as rollers, and cross-channel (lateral shock) waves may or may not be present as diagonal waves that roughly attach to the sidewalls of channels (see Chanson, 2009; Ohtsu

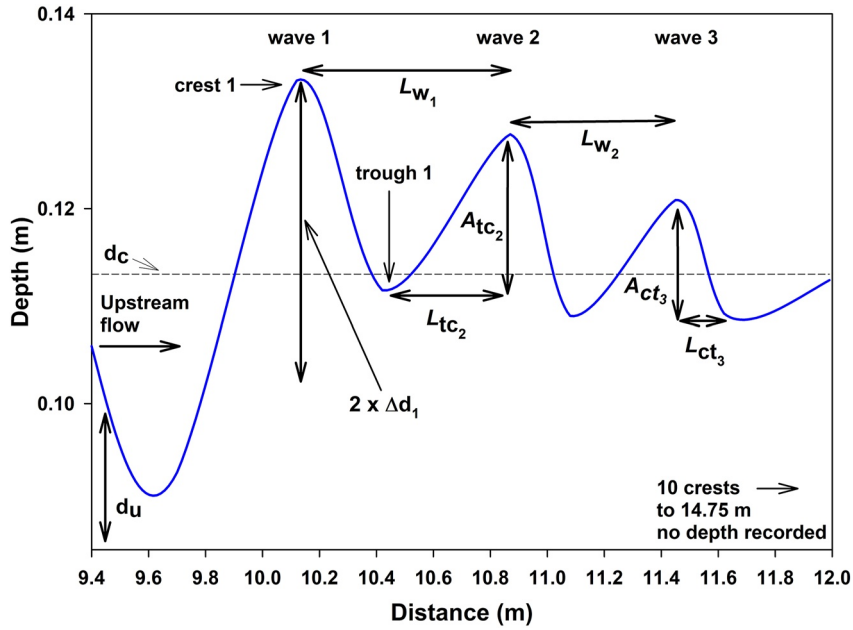

Figure 2. Longitudinal profile of an undular hydraulic jump with definitions and dimensions, based on representative experimental run HCUJ4b (Chanson, 1995). The upstream approach flow has Froude number (Fr) = 1.1. Note wave asymmetry with lee (downstream) side steeper than stoss (upstream) side. Refer to Table 1 for variable definitions (also see Figure 2 in Chanson and Montes (1995)).

et al., 2003). From experimental and field observations, undular hydraulic jumps form when the flow immediately upstream of the wave train is near, or slightly above, critical flow ($1 \leq Fr \leq \sim 2$). Above $Fr > \sim 1.5$ to 2.0, free-surface undulations begin to dampen and disappear, with no undulations observed above $Fr \sim 2.9$ (Chanson & Montes, 1995). Like all hydraulic jumps, undular hydraulic jumps are a fundamental hydraulic mechanism for dissipating energy as flows transition from supercritical ($Fr > 1$) to subcritical ($Fr < 1$) conditions. Unlike single,

Table 1
Definition of Variables Used in Water and Lava Flow Analysis

Variable	Definition
d	Flow depth measured perpendicular to the channel bottom (m)
d_u	Flow depth measured upstream of undular hydraulic jump wave train (m)
L_{wx}	Wavelength (crest-to-crest or trough-to-trough) for the xth wave number (m)
L_c	Wavelength (crest-to-crest) (m)
L_t	Wavelength (trough-to-trough) (m)
L_{tcx}	Length from trough to crest for the xth wave number (m)
A_{tcx}	Amplitude (difference in height) from trough to crest for the xth wave number (m)
L_{ctx}	Length for crest to trough for the xth wave number (m)
A_{ctx}	Amplitude (difference in height) from crest to trough for the xth wave number (m)
Δd_x	½ amplitude (~average of A_{ctx} and A_{tcx}) for the xth wave number (m)
g	Gravitational acceleration (9.80 m/s^2)
q	Specific discharge, water discharge per unit width (m^2/s)
U	Mean velocity (m/s)
U_{max}	Maximum surface velocity (m/s)
S	Channel slope (m/m)
d_c	Critical flow depth for a rectangular channel: $\sqrt[3]{\frac{q^2}{g}}$ (m)

stationary hydraulic jumps, however, energy dissipation in undular hydraulic jumps occur over an extended wave train rather than in a solitary wave.

Kennedy's (1960, 1961, 1963) fundamental work on undular hydraulic jumps in mobile bed streams focused on the coupling between antidune formation on the bed surface and the corresponding stationary waves on the water surface. His theoretical formulation rested on the hypothesis that "… the flow will seek out the wavelength for which fluid motion … will have the minimum energy (Kennedy, 1960, p. 20). He further states that "Under this hypothesis, flow over antidunes is the same as the segment of flow above an intermediate streamline of the fluid motion associated with stationary gravity waves (*waves with celerity equal and opposite to the flow velocity*)." (Emphasis added). Note that this hypothesized condition is precisely the definition of critical flow. Under these conditions, Kennedy (1960, 1963) showed that the antidune and corresponding stationary wavelength scaled with flow velocity as:

$$L_w = 2\pi U^2/g \tag{2}$$

This relation was confirmed experimentally (Kennedy, 1960, 1961, 1963).

At critical flow, where $Fr = 1$ and thus $d = U^2/g$, Equation 2 can be written as a function of depth (d):

$$L_w = 2\pi d. \tag{3}$$

This work was extended using measurements of undular hydraulic jumps in steep ($S > 0.01$), mobile, sand-bed coastal streams (Figure 1a), where Grant (1997) proposed that high-energy rivers tend to adjust toward critical flow ($Fr = 1$) as a balance between forces accelerating the flow and those extracting energy and momentum from it. At-a-point measurements showed that flows locally alternated between supercritical and subcritical conditions, with the channel centerline average very close to $Fr = 1$. Recent flume experiments have largely confirmed this hypothesis and extended it to coarse bed channels (Piton & Recking, 2019).

Empirical field studies have demonstrated that, under conditions of critical flow, Kennedy's (1960, 1963) relation (Equation 2) can be extended to channels with fixed, immobile beds as well. Velocities predicted from Equation 2 and field-measured wavelengths of undular hydraulic jumps in a rock-bed channel correlated with field measurements of flow velocities with an R^2 of 99.9% (Tinkler, 1997). To further explore whether and where Kennedy's relation can be reliably applied to fixed-bed channels, and therefore potentially to lava flow channels, we drew on flume data from Chanson's (1995) experiments using a fixed bed.

2.3. Analysis of Undular Hydraulic Jumps in Water Flume Experiments

We first evaluate undular hydraulic jump theory, and test Kennedy's (1960, 1963) relation (Equation 2), using data collected in fixed-bed flume experiments with water. We extracted data on wave characteristics and hydraulic conditions from Chanson's (1995) experiments in which detailed measurements of flow depth and velocity allow us to calculate Fr at wave crests and troughs longitudinally along the flume for the first few waves of the undular wave trains (Text S1 in Supporting Information S1). Of particular note, Chanson's experiments were conducted in a flume having constant width, constant slope, a smooth bed with no abrupt changes in elevation, and smooth sidewalls. As a result, the experiments did not contain any abrupt change in slope, bed elevation, channel width, or a deformable bed to force the formation of undular hydraulic jumps. The resulting undular hydraulic jumps in these experiments occurred solely because the flow was supercritical upstream and subcritical downstream, thereby forcing a hydraulic transition that produced the jumps.

Chanson and Montes's (1995) data reveal clear patterns in depth, velocity, and Fr not previously reported (Figure 3). Depth measurements show that the undular form of the waves and crest depths remain nearly constant, and greater than critical flow depth, throughout the first several waves in the train. Flow depths in the troughs of the wave train, however, quickly level off at critical depth (Figure 3a). Here, critical depth (d_c) is calculated from the mean upstream approach velocity and depth in a rectangular channel as:

$$d_c = \sqrt[3]{\frac{q^2}{g}} = \sqrt[3]{\frac{(U d_u)^2}{g}} \tag{4}$$

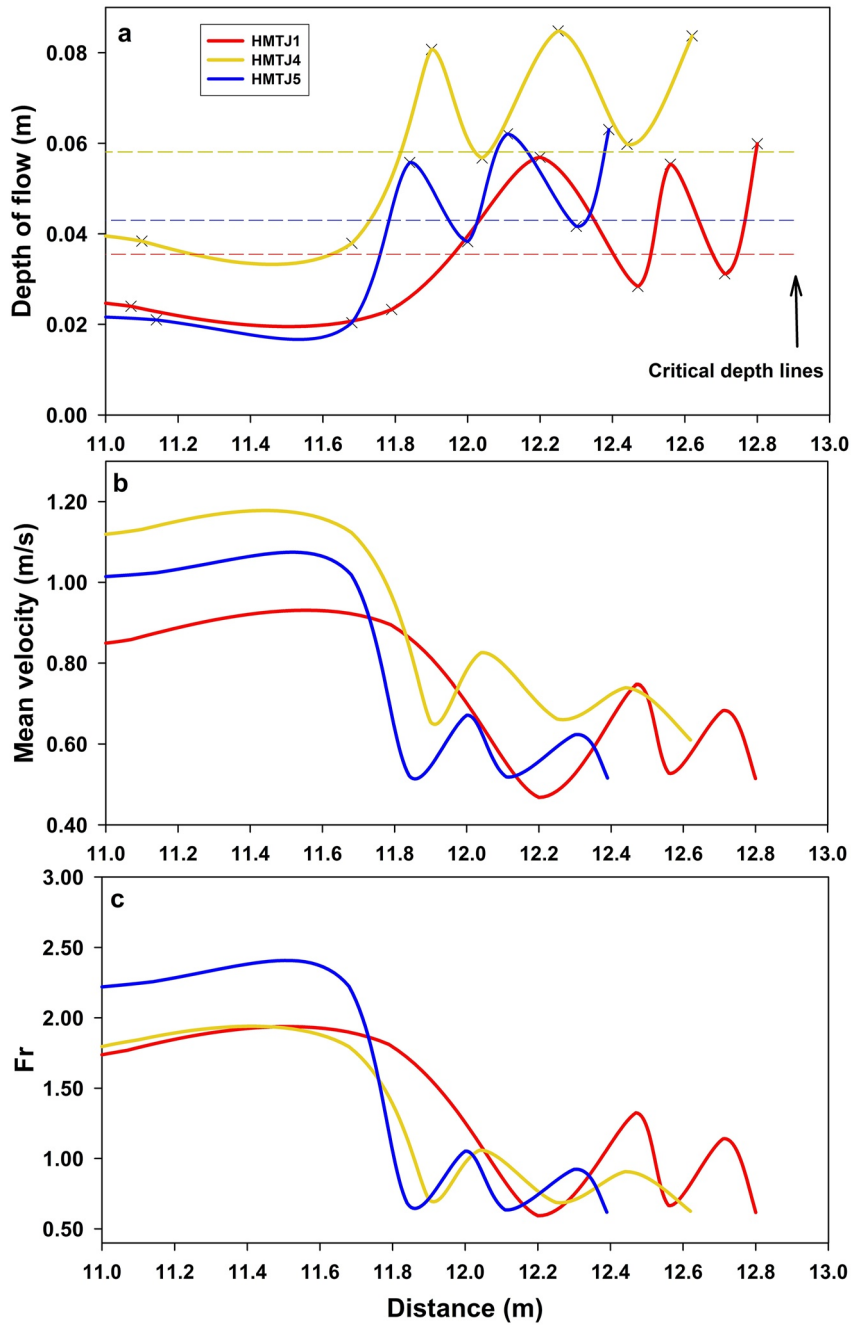

Figure 3. Three representative undular hydraulic jumps from Chanson's (1995) HMTJ series of experiments where depth and specific discharge were measured for the upstream flow and for the first three crests and two troughs of each wave train. Experimental runs varied in their initial conditions (slope and discharge) in order to generate different approach Fr. (a) Profile view of flow depth versus distance from head of flume. (b) Mean velocity versus distance. (c) Froude (Fr) number versus distance.

where q is specific discharge, U is upstream flow velocity, and d_u is upstream flow depth (Chanson, 1995; Henderson, 1966). Chanson (2009) showed that wavelength (L_w) scaled by upstream approach depth (d_u) varied by Fr, increasing from $L_w/d_u \sim 6$ to 8 at $Fr = 1$ to $L_w/d_u > 10$ for $Fr > 2$.

As depth varied through the wave train, flow velocity of both crests and troughs decreased markedly with distance along the flume yet retained a nearly constant velocity difference between crests and troughs (Figure 3b). These

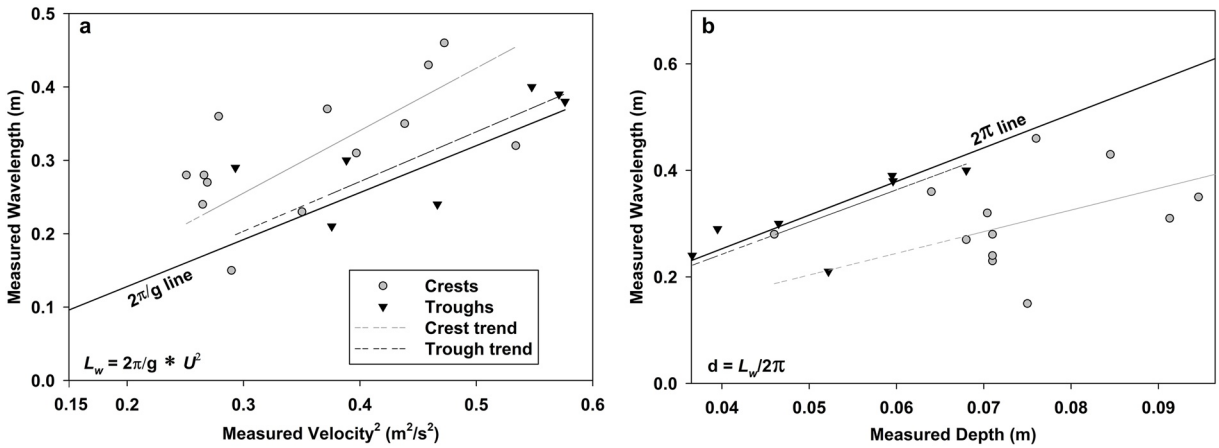

Figure 4. Empirical tests of key predicted relations for undular hydraulic jumps using Chanson's (1995) data. Legend applies to both plots. All trends lines have been fitted through the origin. (a) Relation between wavelength and velocity; the proportionality line is the relation predicted by Equation 2. Crest trend line has a slope of 0.85 and r^2 of 0.23. Trough trend line has a slope of 0.67 and r^2 of 0.47. (b) Relation between wavelength and flow depth; the proportionality line is the relation predicted by Equation 3. Crest trend line has a slope of 4.07 and r^2 of 0.01. Trough trend line has a slope of 6.06 and r^2 of 0.54.

data reveal that *Fr* rapidly converged to the critical state by the second or third wave, varying slightly between the crests and troughs for subcritical and supercritical flow, but averaging very close to $Fr = 1$ (Figure 3c). This convergence occurred even when the upstream flow was strongly supercritical ($Fr \sim 2$). Wavelengths also remained relatively constant after the first wave. Eventually, *Fr* declined to a subcritical value, highlighting that the wave train as a whole dissipates energy from the fluid.

We tested Kennedy's (1963) theory relating wavelength to velocity by comparing measured mean velocities along the wave train with those calculated using measured L_w and Equation 2; the position for each wavelength was assigned to the measurement endpoint for each crest or trough. Along the first few waves, where *Fr* converges toward $Fr \sim 1$, the proportionality constant between L_w and U^2 for all measurements is 0.60 ± 0.03, in good agreement with the theoretical proportionality constant of 0.64 ($2\pi/g$; Figure 4a, Text S2 in Supporting Information S1). This close correspondence to the theoretical proportionality indicates that estimates of hydraulic parameters such as velocity and flow depth based on wavelength over a fixed bed and assuming critical flow are valid. The closest correspondence was for the trough portion of the wave trains (Figure 4a), which likely occurs because of the oscillating nature of flow in undular hydraulic jumps. The flow decelerates and becomes subcritical locally in the crests and accelerates and converges to critical or slightly supercritical in the troughs, where it is close to critical depth (Figure 3a).

Wavelengths of crests and troughs are highly correlated within individual wave trains ($L_t/L_c \sim 1$; Text S3 in Supporting Information S1) and *Fr* is closest to 1 in wave troughs versus wave crests (Table S1 in Supporting Information S1). Estimates of flow depth based on wavelength and an assumption of critical flow (Equation 3) show excellent agreement with measured depths of troughs for both L_t and L_c across the first few waves (*p*-value 0.016; Figure 4b, Text S4 in Supporting Information S1). Based on the strength of Kennedy's (1963) relation for both mobile-bed and fixed-bed flows at critical state, we next explore whether the same correlations apply to lava flows and channels where, as we show, the bed is likely fixed.

3. Properties, Observations, and Measurement of Hawaiian Lava Flows

With a history of long-term monitoring and frequent effusive eruptions, Hawai'i has been used as a laboratory to study the physical and chemical properties of lava flows as well as controls on their emplacement (Cashman & Mangan, 2014). Large effusive eruptions are the most hazardous because high effusion rates are associated with high initial rates of lava flow advance and long distance of travel (Kauahikaua et al., 2003; Pinkerton & Wilson, 1994; Rowland & Walker, 1990; Walker et al., 1973). The correlation between effusion rate and flow behavior is a consequence of competition between flow advection and cooling (Griffiths, 2000), since cool-

ing results in the formation of a (restraining) surface crust and significant crystallization of the flow interior (Cashman et al., 2006; Griffiths et al., 2003; Riker et al., 2009). Volumetric effusion rate (VER) at the vent can be approximated as:

$$\mathrm{VER} = \frac{2}{3} U_{\max} d w \tag{5}$$

where $U_{\max}$ is the maximum surface velocity, d is flow depth and w is flow width. This formulation assumes a channel cross-section that is wide relative to flow depth, consistent with observations of drained channels, and that mean velocity $U = 2/3\ U_{\max}$ (which assumes Newtonian flow down an inclined plane; Bird et al., 2007). In Hawai'i, lava exiting the vent is typically hot and crystal-poor (low viscosity), allowing an assumption of Newtonian behavior although high near-vent bubble contents may cause shear-thinning (Birnbaum et al., 2021; Llewellin & Manga, 2005; Mader et al., 2013; Rust & Manga, 2002). Where flows comprise numerous channel branches, flow data must be obtained for all active branches to compute total effusion rate (Dietterich & Cashman, 2014). VER can be converted to either dense rock equivalent (DRE) or mass eruption rate by measuring the vesicularity (density) of near-vent samples (typically ~60 to 80 volume % or 500–1,000 kg/m^3; Lipman & Banks, 1987; Patrick et al., 2019; Riker et al., 2009).

Historical airborne and ground-based measurements of surface velocities and channel widths are now being augmented by innovations in video analysis to provide new constraints on flow characteristics, including calculation of mean velocity from surface velocity profiles and improved estimates of channel cross-section geometry (Lev et al., 2012; Lev & James, 2014). Surface velocities are typically highest near the vent, such as $U_{\max}$ >17 m/s measured in the near-vent channels of the 1984 Mauna Loa lava flow (Lipman & Banks, 1987). High velocities can also be observed downflow, an example being where the 1950 Mauna Loa flow cascaded over topographic breaks (Finch & Macdonald, 1953).

The most challenging measurement for effusion rate estimates, however, is that of channel depth. Channel depth and geometry are commonly obtained from drained channels after an eruption has ended. These depths are minima where channel drainage is incomplete (Calvari et al., 2003; Dietterich et al., 2018; Lipman & Banks, 1987; Rhéty et al., 2017) or maxima in lava tubes, where thermal erosion is common (Kauahikaua et al., 1998). In real time, minimum flow depths have been estimated from observations of lava "boats," large pieces of collapsed channel levees that are carried within lava streams and assumed to be less dense on average than the lava in the channel, so that their height above the flow surface approximately equals that below the surface (Lipman & Banks, 1987). In high effusion rate Hawaiian lava flows, near-vent flow depths estimated from lava boats are typically about 5 m. Channel depth can also be modeled from observations and estimates of other flow parameters using Jeffreys' (1925) equation for shallow flow (width w >> depth d):

$$d = \sqrt{\frac{3U\mu}{\rho g \sin\alpha}} \tag{6}$$

where sin α is the flow-surface slope. Whereas velocity can be measured and slope can be approximated from the channel topography, viscosity must be estimated from textural and geochemical properties (e.g., Harris et al., 2017; Mader et al., 2013) or from flow dynamics (Lev et al., 2012; Tallarico & Dragoni, 1999).

Another approach to estimating depth of lava flows comes from hydraulics, specifically from the observation of standing waves (Le Moigne et al., 2020). Lava flows exhibiting such waves have high surface velocities and have been described as being "… like that of a large river of water in flood" (Macdonald, 1943). Standing waves reached amplitudes of 0.9–1.2 m (3–4 ft) in the 1942 Mauna Loa lava flow where $U_{\max}$ was 6.7–8.9 m/s (15–20 mi/hr; Macdonald, 1943) and up to 3.7 m (12 ft) in the high-velocity lava flows of 1950 ($U_{\max}$ of 11.2–13.4 m/s or 25–30 mi/hr; Finch & Macdonald, 1953). Standing waves have also been observed in channels and lava tubes at the bases of lava falls (Kauahikaua et al., 1998; Richter et al., 1970) and other elevation drops or slope changes in low viscosity, high velocity flows (Geist et al., 2008; Wolfe, 1988). These reports of standing waves in lava may, however, reflect some confusion in nomenclature, since both stationary hydraulic jumps and undular hydraulic jumps are types of standing waves. Without clear discrimination between these two styles of waves, this distinction is lost by using the more generic term "standing wave."

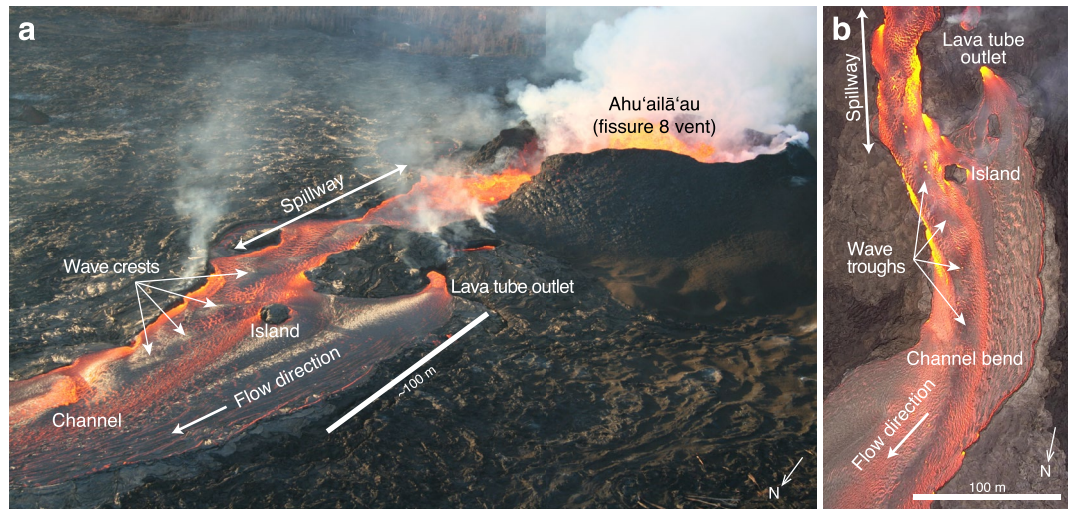

Figure 5. Overview of the Ahu'ailā'au cone (fissure 8) and proximal lava channel morphology and undular hydraulic jump wave train during the 2018 lower East Rift Zone eruption of Kīlauea volcano, Hawai'i. (a) Oblique aerial photo looking southeast taken on 20 June 2018. (b) Nadir UAS video frame from 24 June 2018.

Extension of hydraulics of open-channel water flow to behavior of lava flows rests in part on whether the hydraulics of concern generate solitary standing waves or trains of standing waves (undular hydraulic jumps). Le Moigne et al. (2020) used theory developed for individual hydraulic jumps (solitary stationary waves) to extract lava flow parameters. Here, we take a complementary approach by testing the applicability of hydraulic theory developed for undular hydraulic jumps in water to basaltic lava flows.

4. Measurements of Undular Hydraulic Jumps in the 2018 Kīlauea Lava Flow

4.1. Undular Hydraulic Jump Observations During the 2018 Eruption of Kīlauea Volcano

The 2018 eruption of Kīlauea volcano produced exceptional undular hydraulic jumps in the form of extended wave trains (Dietterich et al., 2021; Neal et al., 2019; Patrick et al., 2019) (Figure 5). The 2018 eruption started on 3 May 2018 as a fissure eruption in the lower East Rift Zone of the volcano, fed by a dike intrusion from up-rift. Although individual flows were short-lived early in the eruption, the introduction of hotter, more mafic magma to the rift zone on ~17 to 18 May fed larger and more vigorous flows that reached the ocean on 19 May (Gansecki et al., 2019; Neal et al., 2019). On 28 May, activity became focused at a single vent (fissure 8, or Ahu'ailā'au), which remained active until the eruption waned in early August 2018. By the end of August, 0.9–1.4 km^3 DRE of lava had erupted, with 0.4 km^3 deposited on land and at least 0.5 km^3 offshore (Dietterich et al., 2021).

The fissure 8 vent (Ahu'ailā'au) fed a persistent channel with a near-uniform slope that was monitored for flow velocity, stage (channel fill level) fluctuations, and surficial flow features using repeat UAS observations at specified stations (Dietterich et al., 2021). These data provide a time series of maximum surface velocities including, in mid to late July, variations in near-vent flow velocities from ~5 to 15 m/s over timescales of minutes (Patrick et al., 2019). Channel widths, in contrast, remained stable at ~30 m in the proximal spillway and ~75 m in the proximal channel that we examine here (Figure 5). Lava-flow density in this proximal reach was about 900 ± 200 kg/m^3 (71% ± 4% vesicularity; Patrick et al., 2019). Data from this reach were used by Dietterich et al. (2021) with analytical theory of channelized flow (Equations 5 and 6) to create a time series of instantaneous lava effusion rates.

The appearance and amplitudes of the observed waves (Figure 5, Movie S1) fluctuated as a function of volumetric flux. Spatial positions of the waves remained relatively stable but could expand over distances in excess of one hundred meters as flux rate varied. Amplitudes fluctuated by as much as a couple of meters. For example, during an episode of pulsing activity in mid to late July, wave amplitudes grew and diminished with velocity fluctuations

over 5–10 min (Patrick et al., 2019). At the same time, the dimensions of single waves appeared to compress and relax in amplitude and to shorten and elongate back to front (Movie S2), while wavelengths increased and waves propagated farther downflow at high flow (Movie S3). Unlike undular waves in water flow, however, the waves in the lava flow never grew to the point that they became breaking or roller waves. An exception is the lava behavior where it emerged from the vent and traveled through a narrow spillway (Figure 5); here the exceptional flow velocity combined with the curvilinear channel geometry caused the lava to forcefully impinge on channel margins, which caused the flow to churn and overturn. This churn created a splashy appearance to the overall flow behavior, triggered cross waves (shock waves), and generated infrasound analogous to breaking water waves (Lyons et al., 2021). Below the spillway, the flow widened (Figure 5). Widening, together with the high viscosity of the lava and growth of minor surface crust, created trains of undular waves that were smooth and appeared laminar with little to no visible churning. Lack of turbulent churning also damped generation of acoustic energy. As a result, despite moving at velocities to a few tens of meters per second and developing undular waves having amplitudes of as much as two or more meters in height, passage of the lava flow was notably quiet below the spillway (Movie S1).

4.2. 3-D Imaging of Undular Hydraulic Jumps

Measurements of wave trains in the active lava channel were made possible by regular channel monitoring with airborne remote sensing (Desmither et al., 2021; Dietterich et al., 2021; Lyons et al., 2021; Patrick et al., 2019). Airborne lidar captured elevation data from the lava-flow surface proximal to the vent between 8 and 12 July 2018 (USGS, 2018a, 2018b; available on OpenTopography). Over this period, three sets of wave-train point clouds can be extracted: 8 July at ∼14:00 HST (Hawaiian Standard Time), 10 July at ∼10:00 HST and 12 July at ∼13:00 HST (Figure 6). Point clouds were post-processed into bare-earth 0.5-m-resolution DEMs. Post-eruption 0.25-m-resolution lidar of the drained lava channel flown 17–26 July 2019 revealed a rectangular channel cross-section (Mosbrucker et al., 2020). Profiles of all elevation data were extracted downstream from the vent along the channel axis to capture the wave forms. Post-eruption lidar data were subtracted from syn-eruption lidar data to estimate flow depth during the eruption, as pre-eruptive lidar data do not capture the lava flows that filled this area prior to channel formation (Figure 7a; Dietterich et al., 2021). This is the best available estimate of active lava depth, but it is uncertain given the possibility of incomplete post-eruption drainage or thermal erosion of the channel floor (Harris et al., 2007). We note, however, that near-vent lava at the end of the eruption remained fluid, facilitating drainage, and flow stage did not trend lower over time during the eruption in a way that would suggest significant thermal erosion (Dietterich et al., 2021). To reduce noise, all data sets were processed with median filtering. The lidar snapshots of the wave trains on three separate days (8, 10, and 12 July) were used to obtain direct measurement of wavelengths and amplitudes as a function of distance from the vent. Gaps in the profiles result from gaps in the lidar point clouds (Figure 6). Crests and troughs are identified from local maxima and minima and distance from the vent for each wavelength measurement is assigned the downstream position of the crest or trough in a measured pair. These data, along with depth from lidar differencing, provide a full complement of information with which to test hydraulic relations.

4.3. Channel Video Analysis

Video and imagery acquired from UAS were used to quantify wave-train locations, wavelengths, and the corresponding surface velocity field in the near-vent lava channel. Short (1–10 min) overhead (nadir) video was acquired regularly over the course of the eruption using DJI Matrice 600 and Mavic Pro UAS (Desmither et al., 2021; Dietterich et al., 2021). Video frames were scaled for analysis using features along the channel margins in other geospatial data collected at similar times, such as airborne imagery and lidar. Unfortunately, no video recording occurred within ∼5 hr of each lidar survey, thus we cannot specifically match 3-D waveforms to velocities. Nevertheless, we analyzed video from the broad time period over which lidar data were acquired, a period that represents a range of volumetric flow rates.

Troughs and crests throughout the wave trains were identified in video and still images based on their variable crust coverage and incandescence (Figure 7b). Wavelengths were measured from trough to trough and crest to crest where identifiable. Flow varied throughout the eruption and analyzed videos included periods of both steady

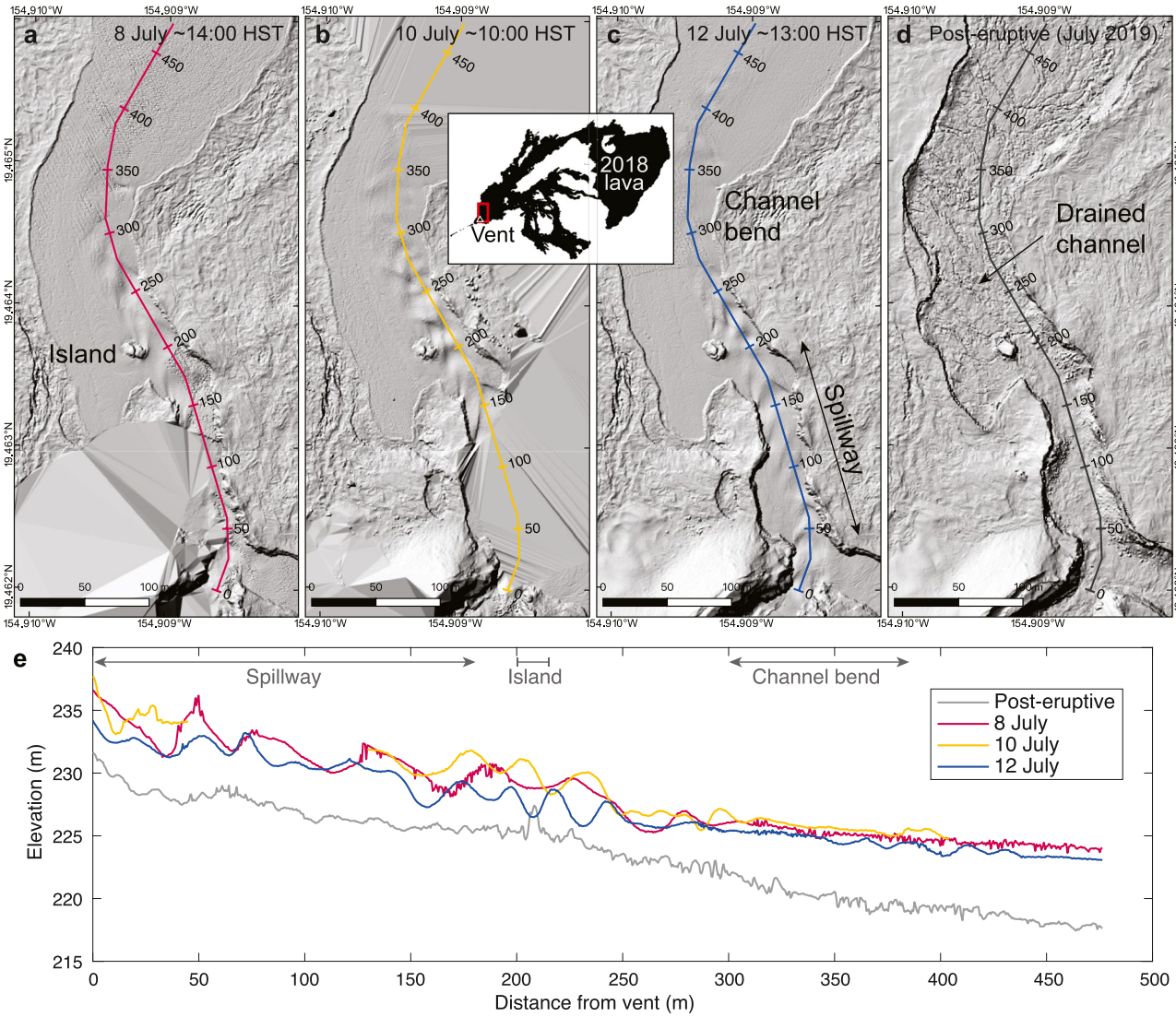

Figure 6. Wave trains captured in the surface topography of lava flow by syn-eruptive lidar surveys 8–12 July 2018. (a) 8 July lidar hillshade. (b) 10 July lidar hillshade. (c) 12 July lidar hillshade. (d) July 2019 post-eruptive lidar hillshade. Numbers indicate distance from vent (m). (e) Elevation profiles of all syn-eruptive lidar and the post-eruptive lidar data. Note that although there are local variations, channel bed slope is nearly constant; there is no abrupt break in slope that would obviously trigger formation of undular or solitary hydraulic jumps. Inset shows reference map of the 2018 lava flow field and the location of the fissure 8 vent (Ahu‘ailā‘au).

flow and short-period “pulsing” (Patrick et al., 2019; Movies S2 and S3). Under steady flow conditions, measurements were made from representative video frames; when flow in the channel was pulsing, video measurements were made from frames extracted every 15 s.

Particle Image Velocimetry with PIVlab (Thielicke & Stamhuis, 2014) was used to extract the surface velocity field from each video. Data were sampled along down-channel profiles centered along the maximum velocity and wave-train axes and averaged for all time steps during steady flow (Figure 7c). When velocity was variable, we used median filtering with a 5-s window to calculate the surface velocity at times corresponding to the wave measurements. No syn-eruptive flow depth measurements were possible. Flow depth, and thus *Fr*, for these video acquisitions of the lava flow are therefore estimated from velocity following Jeffreys' (1925) viscous-shallow-flow theory (Equation 6) using a flow density of 900 ± 200 kg/m^3 (from analysis of channel samples ~130 m from vent) and viscosities of 200 ± 100 Pa s (Dietterich et al., 2021; Patrick et al., 2019). Flow depths estimated using Equation 6 are consistent with those made from lidar differencing and the depth range agrees with ground-based observations of variable flow stage (Figure 7a; Patrick et al., 2019).

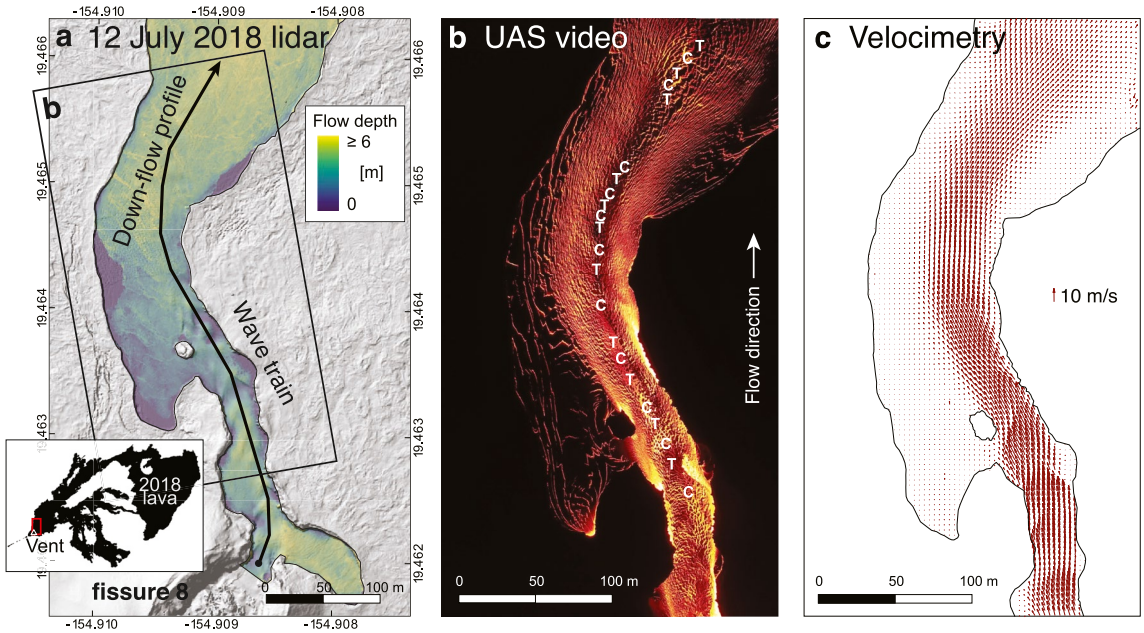

Figure 7. (a) 12 July lidar hillshade with flow depth from differencing against the post-eruptive lidar DEM. Thin margins and zero-thickness regions owe to late-stage channel morphology changes, but the thickness within the wave train is not affected (Dietterich et al., 2021). (b) UAS video frame (extent shown in panel (a)) with wave crests and troughs labeled (C, crest; T, trough). (c) Velocity field extracted from particle velocimetry processing of the UAS video in panel (b).

5. Results From Analysis of 2018 Kīlauea Lava Flows

5.1. 3-D Lidar Imaging of Wave Trains

Undular hydraulic jump profiles show that flow depths, wavelengths, and amplitudes varied with flux rate and distance from the vent at different acquisition dates and times (Figure 8, Table S2 in Supporting Information S2). Relatively high effusion rates on 8 and 10 July produce depths of 4–6 m and wavelengths ≤60 m whereas lower effusion rates on 12 July produced flows with depths of 2–5 m and wavelengths ≤~40 m. Wave amplitudes are greatest (~2 m) between 150 and 250 m from vent, corresponding to the channel reach adjacent to an island formed in the flow (Figure 6); they decrease to ~0.5 m at >300 m from vent. The waves are approximately symmetric, without any apparent skew (Figure 8).

5.2. Channel Video Analysis

Videos from 24 June and 8, 11, and 19 July capture maximum velocities that decay down-flow from ≤17 m/s at 150 m from vent to ≥2.5 m/s at nearly 500 m from vent (Figure 9, Table S3 in Supporting Information S2). Along the undulating wave train, velocities peak near wave troughs where the crust is compressed and dark and are slower at the wave crests where the crust extends, revealing more incandescence (Figures 7 and 9). This velocity oscillation decays with distance from vent in parallel with a decrease in wave amplitudes seen in the lidar data (Figure 8c). Measurements of the 19 July flow, collected during a "surge" in effusion (Patrick et al., 2019), yield higher velocities and little wave development. Depths calculated from Equation 6 range from 3 to 6 m (Figure 9a), within the range of those observed by differencing of DEMs obtained during the 8–12 July flow period (Figure 8a). *Fr* based on measured velocities and estimated depths are near or above critical (~0.8 to 1.6) within the first ~400 m (Figure 9b). Observable waves occur only where *Fr* is near critical (~0.8 to 1.3), including a single wave in the 19 July video at the end of the measurement reach 450 m from the vent (Figure 9d), as *Fr* drops toward 1. *Fr* becomes subcritical and decays with distance beyond the wave trains.

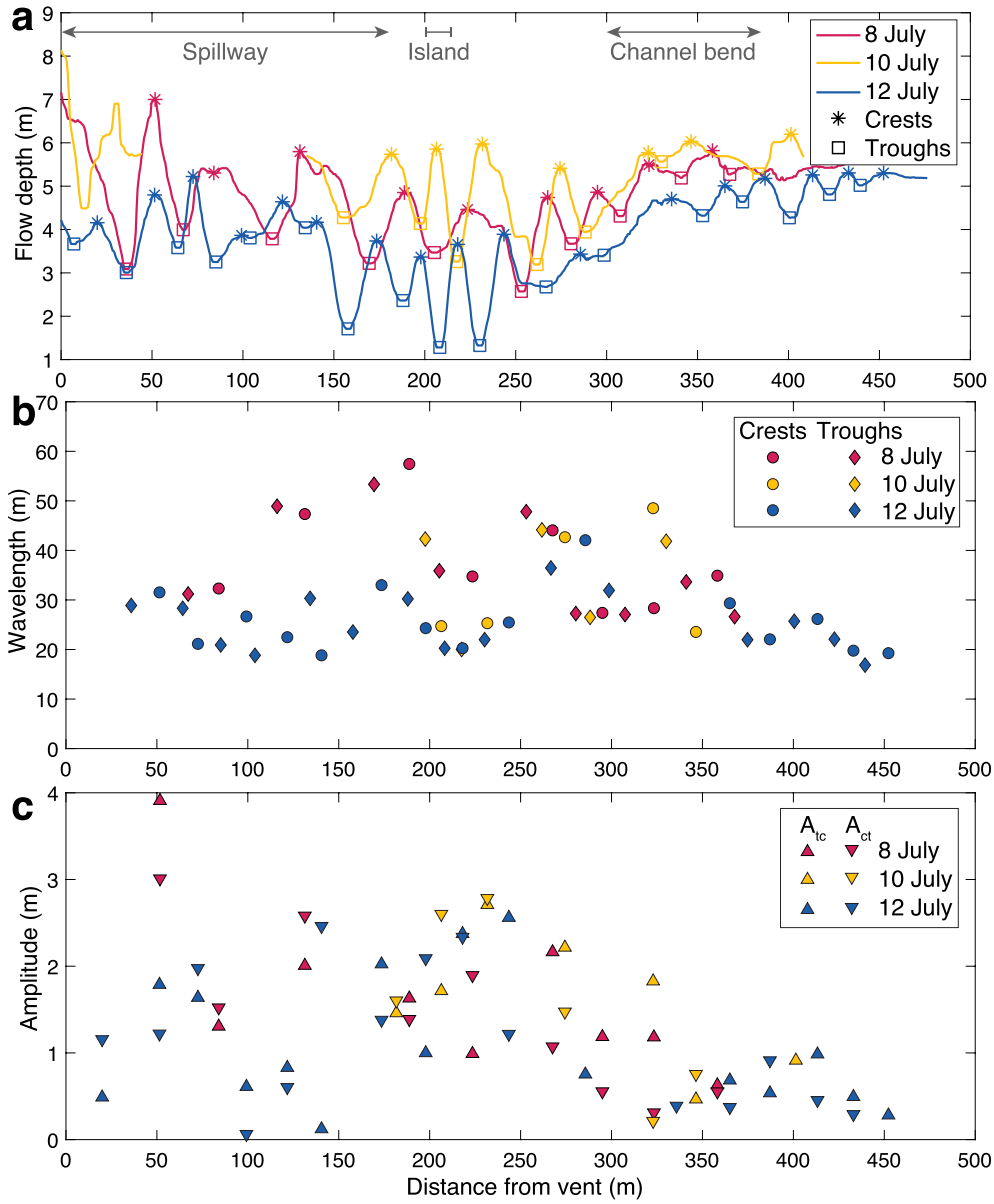

Figure 8. Wave measurements versus distance from vent at different lidar acquisition times (Figure 6). (a) Depth of flow from surface elevation relative to the post-eruptive channel elevation (Figure 6). Crests and troughs determined from local maxima and minima. (b) Crest-to-crest (L_c) and trough to trough (L_t) wavelengths versus distance from vent. (c) Amplitudes on the upstream (A_{tc}) and downstream (A_{ct}) sides of waves versus distance from vent.

5.3. Comparison of Observed Lava Flow Wave-Train Wavelengths With Theoretical Predictions

For near-critical flows, wave-train wavelengths (L_w) are expected to scale as mean velocity squared (Equation 2; Kennedy, 1963). Examination of Figure 9 shows that the Kīlauea 2018 lava flow remained at near-critical conditions to ~500 m from the eruptive vent. We use UAS measurements of wavelengths and velocities over this distance to test the Kennedy (Equation 2; Kennedy, 1963) relationship (Figure 10a). Similar to the measurements for undular hydraulic jump wavelengths in water, velocity and wavelength in the lava flow are positively correlated. Despite scatter at high velocities, which is reduced by averaging over proximal (<200 m; spillway), medial (150–300 m; wider zone with best wave morphology) and distal (>350 m; after the channel bend) sections of the reach, these data generally follow the expected slope of $2\pi/g$ (~0.64). This clear correspondence between behavior of flows of water (Figure 4a) and lava (Figure 10a) supports the application of critical flow theory to wave trains in lava flows.

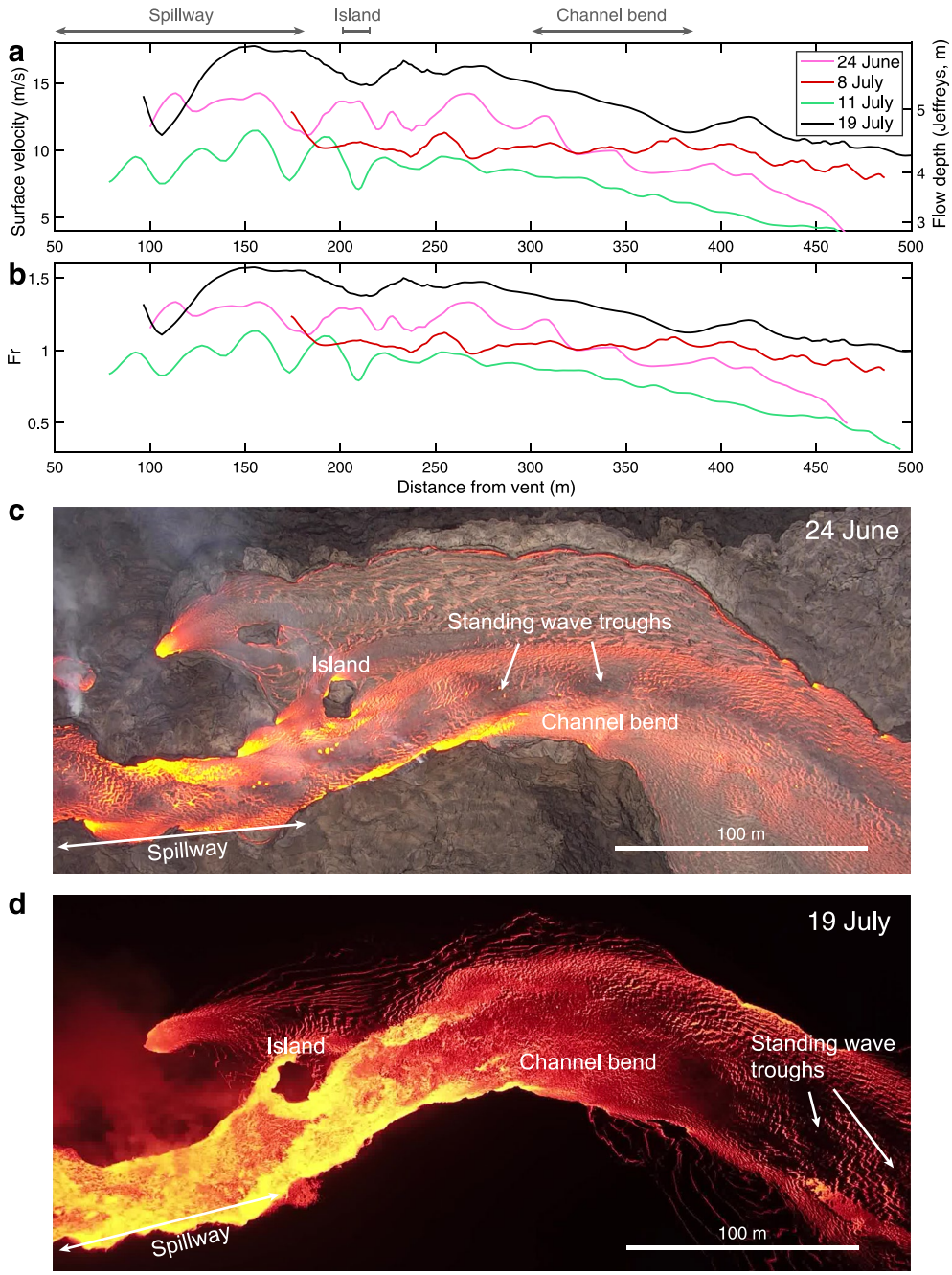

Figure 9. (a) Maximum surface velocity and derived flow depth along proximal channel reach. (b) Froude (Fr) number calculated from depth estimates based on Jeffreys' Equation 6. (c and d) Annotated examples of UAS video frames from 24 June and 19 July (surge) for reference.

We also use lidar measurements of wavelengths and depths estimated from DEM differencing to test the Kennedy (Equation 3) relationship (Figure 10b). The wavelength-to-flow depth relationship shows substantial scatter owing in part to the large amplitudes of the waves. The ratio of wavelengths to flow depths for all waves is 8 ± 4, which is, within uncertainty, close to the predicted value of 2π. However, results vary with distance from the vent. Averaging all wavelengths and depths retains the scatter but shows that the distal portion of the reach most closely matches the expected relation with flow depth. Deviations from the theoretical relation may reflect changes in flow width along the channel and possible restrictions of wave-train location because of width-velocity rela-

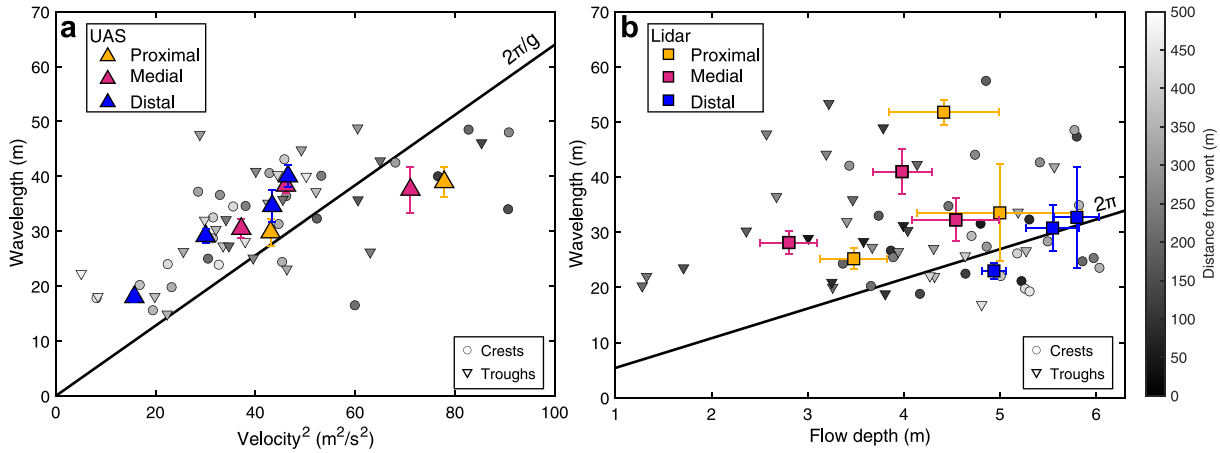

Figure 10. (a) Test of the Kennedy (1963) scaling ($2\pi/g$ line) for the relation between wavelength and velocity. L_t and L_c are plotted relative to the square of the mean flow velocity (U in Equation 2). Grayscale in both plots represents the distance from the vent. Averages are shown for the proximal (<200 m; spillway), medial (150–300 m; wider zone with best wave morphology), and distal (>350 m; after the channel bend) sections of the reach for each survey date. (b) Testing the Kennedy (1963) relationship (2π line; Equation 3) with DEM measurements of flow wavelength and depth. L_t and L_c are plotted relative to depth from lidar differencing.

tions and the requirement of $Fr \sim 1$. Scatter may also reflect underestimated flow depths near the vent due to incomplete drainage. In contrast to the experimental water flows, relations between wavelength and depth for the lava flows appear similar for crest-to-crest and trough-to-trough measurements.

5.4. Flow Conditions That Produce Undular Wave Trains in Lava

We assessed conditions that allow wave-train formation in channelized lava flows. Below the fissure 8 vent (Ahu‘ailā‘au), wave trains formed only when maximum flow velocities (U_{max}) in the channel were ≥6 m/s and they persisted to velocities approaching 15 m/s (Figure 9a). At the high-velocity end, wave-train formation gave way to chaotic, supercritical flow in the highest-velocity zone near the vent (Figure 9d). Here, well-developed wave trains shifted downstream, propagating farther from the vent (Figure 11, Movies S2 and S3). Changes in the distal wave train occurred over a period of minutes during pulsing flow (e.g., Figure 11d). During the highest pulsing-flow velocities, caused primarily by an increase in lava volume owing to increased bubble content (reduced degassing; Lyons et al., 2021; Patrick et al., 2019), the wave train extended to 700 m from the vent and into the wider downstream reach. During lower-flux periods, when the lava was more degassed and denser, the wave train reached only about 400 m from the vent (Figure 11). Wave trains persisted for at least short time periods at velocities as low as ~3 m/s in the wide, distal reach. However, their formation and hydraulic interpretation are complicated by two key factors: (a) propagation of transient pulses of flow downstream, which result in some wave development under highly fluctuating flow rates; and (b) rheological changes caused by fluctuations in lava vesicularity between 50 and 82 vol% (Patrick et al., 2019). Because of these complications, the lack of undular hydraulic jumps in our main study reach where pulsing yields supercritical flow (Movie S2), and the targeted time period of the lidar acquisitions, we do not incorporate these data into our primary analysis (e.g., Figure 10).

The observed velocity range for wave-train formation is similar to conditions reported for wave formation in past Hawaiian eruptions (e.g., Finch & Macdonald, 1953; Lipman & Banks, 1987; Macdonald, 1943). This consistency indicates that in Hawai‘i, where flow slopes are typically ~0.01 to 0.1 m/m (~0.5°–6°), velocities sufficient to form undular wave trains occur primarily when volumetric eruption rates exceed ~200 m^3/s (Dietterich et al., 2021). From a hazards perspective, these flow rates also promote the fastest advancing lava flows (Cashman & Mangan, 2014; Kauahikaua et al., 2003) that most urgently require real-time effusion rate data for lava flow forecasts.

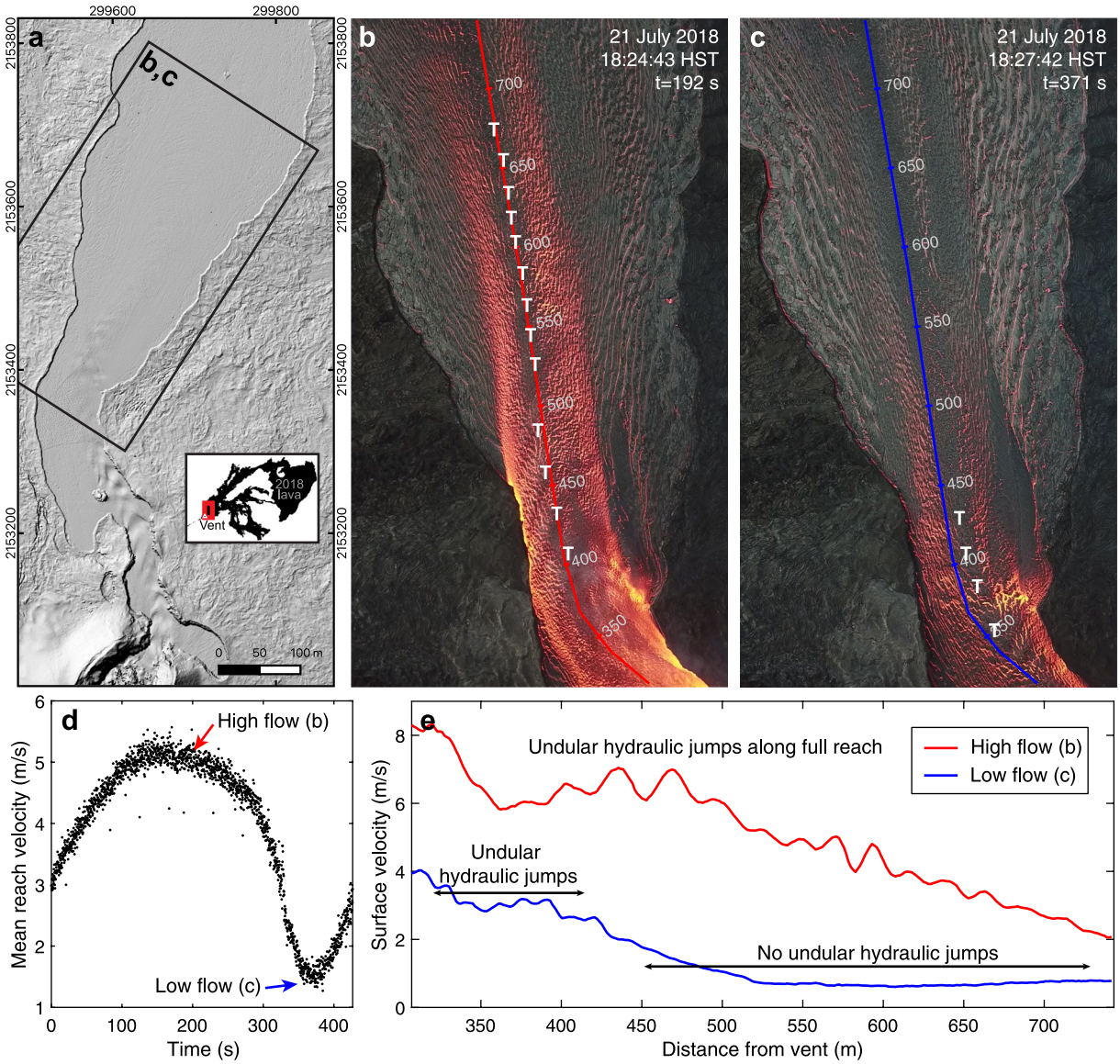

Figure 11. Downflow wave-train propagation during pulsing periods when flow velocity increased and decreased dramatically over minutes (Dietterich et al., 2021; Lyons et al., 2021; Patrick et al., 2019). (a) 12 July lidar hillshade of the proximal fissure 8 channel showing the widening reach past the channel bend and the extent of panels (b and c). (b) 21 July UAS video frame during high flow with distance from vent ticks along the velocity profile line and wave troughs labeled as T. (c) 21 July UAS video frame during low flow with distance from vent ticks along the velocity profile line and wave troughs labeled as T. (d) Mean surface velocity along this reach over the 21 July (18:21 HST) video, annotated with the times of the frames in panels (b and c). (e) Surface velocity profiles at high (b) and low (c) flow.

5.5. Effusion Rates From Undular Hydraulic Jumps

Integrating critical flow theory and our results to calculate VERs (Equation 5) yields valuable, independent measurements of spatiotemporal lava flux (Figure 12, Table S4 in Supporting Information S2). If calculated for each wavelength, however, results from the lidar data (velocity calculated from undular hydraulic jump wavelength; depth measured from lidar differencing) and the UAS data (velocity measured from UAS velocimetry; depth calculated from undular hydraulic jump wavelength) are quite scattered (Figure 12a) although generally consistent, with the highest effusion rates observed during surges on 24 June and 19 July. This temporal variability reflects the large daily cycles in effusion rates (Patrick et al., 2019). Although no UAS survey corresponds directly with the lidar acquisition times, the closest pair from 8 July (~9 hr apart) correspond well. Overall, crest and trough data are more similar in lava than in the water experiments with the main difference (in the lidar data) attributed to the large wave amplitudes and resulting large swings in flow depth (see Figure 8).

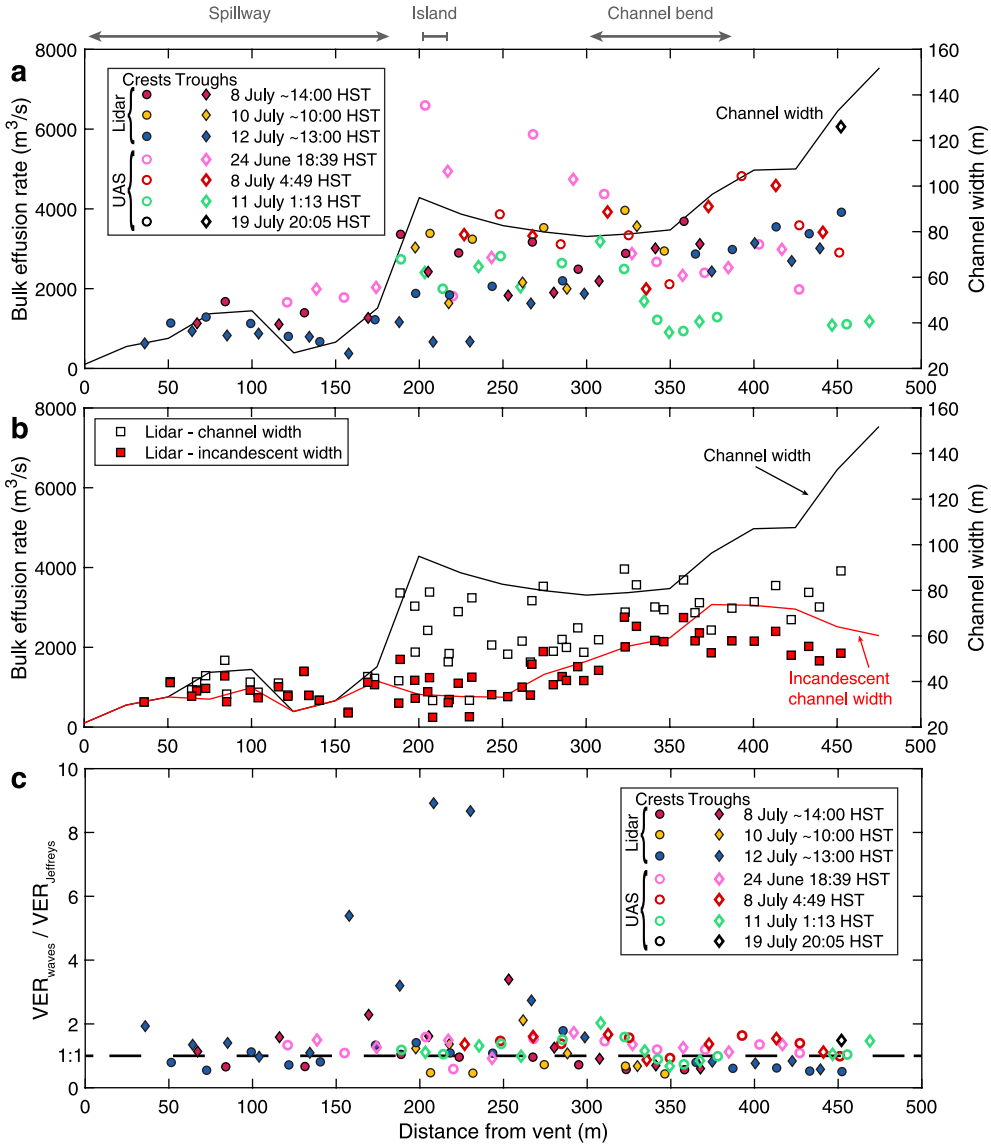

Figure 12. Bulk effusion rate and channel width with distance along the channel. (a) Lidar (filled) and UAS (open) wave-train results for each survey with depth measured from DEM differencing and mean velocity calculated from wavelength ($U = \sqrt[2]{L_w g/2\pi}$) for lidar data and velocity measured from video velocimetry and depth calculated from wavelength ($d = L_w/2\pi$). (b) Comparison of lidar-based bulk effusion rate results using actual and effective channel widths for w in Equation 5: the full lidar-determined channel width (open) and the width of the incandescent portion of the flow measured from UAS data (filled). (c) Ratio of the bulk volumetric effusion rates (VERs) based on depths and velocities calculated from wavelengths (VER_{waves}) and those calculated using Jeffreys' method (Equation 6; $VER_{Jeffreys}$) using the incandescent flow width plotted with distance. The values are mostly similar and cluster around a ratio of 1 (dashed line).

Curiously, we observe an apparently contradictory increase in bulk effusion rate with distance, especially at the end of the spillway (~200 m from the vent) where the channel undergoes a step-wise increase in width (Figure 12b). We note, however, that although the flow widens dramatically at the end of the spillway, the high-velocity, incandescent, undular hydraulic jump-bearing part of the channel remains narrow (Figures 6–9). Using the width of this high-velocity core as measured in the UAS imagery (Figure 12b), rather than the full lidar-determined channel width, removes the apparent stepwise increase in bulk effusion rate and likely produces a more accurate estimate of effusion rate beyond the narrow, confined channel reach. Farther down the channel, the measured effusion rate peaks at the channel bend (~350 m from the vent), which is where the incandescent width spans nearly the full channel width. This apparent increase in flux may be attributable to

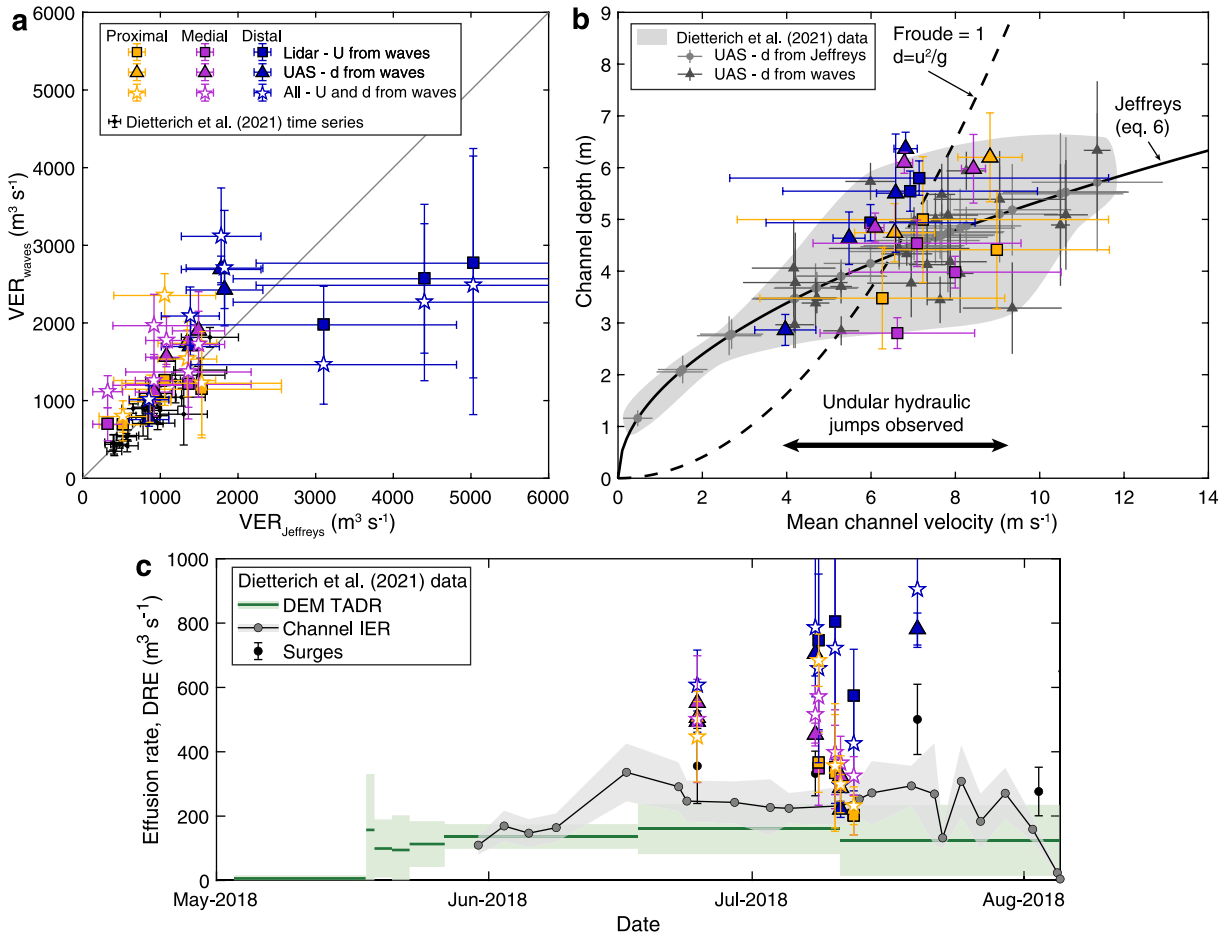

Figure 13. (a) Comparison of bulk effusion rates based on depths and velocities calculated from wavelengths (VER_{waves}) versus those calculated by Dietterich et al. (2021) using Jeffreys' (1925) method ($VER_{Jeffreys}$; Equation 6). (b) Wave-derived depths and velocities; colored symbols from this study, UAS velocity time series data set of Dietterich et al. (2021) shown in gray points and field. The analytical relationship between velocity and depth from the Jeffreys' equation and from wavelength assuming critical flow (Froude number = 1) are plotted for reference. (c) Time series of effusion rates corrected for vesicularity (DRE) that compares results from the 24 June–19 July UAS and lidar measurements to the instantaneous eruption rate (IER) time series estimated from UAS (gray and black symbols) throughout the eruption and time-averaged discharge rates (TADR) from time series topographic data (green bars). IER and TADR data from Dietterich et al. (2021). In all plots, results from this study are averages for the proximal (<200 m), medial (150–300 m), and distal (>350 m) subsections of the reach (see panel a for symbol definitions). Results from the complete UAS time series in Dietterich et al. (2021), are mostly from a location about 200 m from the vent, but they also incorporate proximal and distal locations, including undular hydraulic jumps from more than 350 m distance from the vent during higher flow to maximize temporal resolution.

full merging of a secondary supply of lava from the tubed vent outflow to the west of the spillway (Figure 5). It may also owe to unquantified influences of the channel bend on depth, velocity, and undular hydraulic jump behavior.

5.6. Comparing Effusion Rates Using Critical Flow Assumption and Jeffreys' Equation

Volcanologists have commonly used Jeffreys' (1925) Equation 6 to estimate flow depths and, by extension, VER, from observed channel velocities. We can similarly calculate flow velocities from observed channel depths. When bulk effusion rates calculated using waves from UAS and lidar data (VER_{waves}) are compared to those calculated using this traditional Jeffreys' method ($VER_{Jeffreys}$), we find good agreement (a ratio of VER_{waves}/$VER_{Jeffreys}$ ~1) along the whole reach (Figure 12c). However, we observe outliers in the lidar data for the medial portion of the reach, where the high-amplitude waves record very large and small depths (Figure 8) that yield very high and low velocities in Equation 6, and thus high and low Jeffreys' effusion rates and proportionally lower and higher VER_{waves}/$VER_{Jeffreys}$.

As suggested by Figure 10, averages of effusion rate along subsections of the proximal channel reach are more robust than individual estimates. The proximal subsection (<200 m) represents the narrow, fast-moving spillway that hosts supercritical flow (no undular hydraulic jumps) during periods of highest effusion (e.g., Figure 9d). The medial subsection (150–300 m) has well-formed undular hydraulic jumps in nearly all surveys and sub-reach averaging removes the high and low outliers from the high-amplitude lidar waves (Figure 12c). In the distal subsection (>350 m), after the channel widens and velocity decreases, waves become harder to detect (Figures 8 and 9). When calculated using our data from UAS, lidar, and waves alone, effusion rates in the proximal and medial reaches correspond well with each other, to Jeffreys estimates (Figure 12c), and to the measurements made for the whole eruption time series from UAS data (using velocities at ~200 m and with effusion rates calculated using Jeffreys' method [Equation 6]; Figure 13a; Dietterich et al., 2021). This correspondence demonstrates that estimating relevant flow parameters (depth, velocity) exclusively from wavelengths in undular hydraulic jump wave trains produces results consistent with those based on measured depths and velocities (Figure 13a). This correspondence also demonstrates the power and potential of using measurements from undular hydraulic jumps to extract effusion rate estimates solely from scaled imagery.

In the distal subsection where velocity is calculated from lidar-determined depth, estimates based on Jeffreys' method (Equation 6) yield higher velocities, and thus higher effusion rates, than measurements based on UAS data or extracted solely from wavelengths ($VER_{waves}/VER_{Jeffreys} < 1$; Figures 12c and 13a). These results suggest that the simple wavelength-velocity relation of Kennedy (1963) may provide a better proxy for estimating average flow velocity than does Jeffreys' (1925) which requires estimates of flow depth.

5.7. Comparing Flow Depths Using Critical Flow Assumption and Jeffreys' Equation

Although the Jeffreys' (1925) approach is widely used in volcanology, challenges to the accuracy of this equation include uncertainties in bulk density, bulk viscosity, and slope, all of which may change rapidly along proximal to medial channel reaches and are difficult to measure in real-time. Data shown in Figure 13b from our study (lidar and UAS) and the broader UAS timeseries compiled by Dietterich et al. (2021) can be used to compare the accuracy and precision of depths estimated from Jeffreys' equation and open-channel hydraulic theory for critical flow (Equation 3). Dietterich et al. (2021) estimated flow depths from Equation 6 for all flow conditions and from Equation 3 only when wave trains were present in the channel and flow was assumed to be near-critical (gray points and area in Figure 13b). Although depth estimates show substantial scatter using both approaches, overall error estimates on flow depths (and, as a consequence, bulk effusion rates) are larger using Equation 6 (standard deviation $\sigma = \pm 1.2$ m and ± 424 m^3/s) than when using wavelengths and Equation 3 ($\sigma = \pm 0.7$ m and ± 128 m^3/s).

In contrast to the UAS data, uncertainties in mean flow velocity calculated using depth and undular hydraulic jump wavelength measured by lidar ($U = \sqrt[2]{L_w g/2\pi}$) are large (squares in Figure 13b) compared with errors from UAS velocimetry (triangles in Figure 13b), demonstrating the value of velocimetry data to more precisely constrain effusion rate estimates. Where undular hydraulic jumps are present (4 m/s $\lesssim$ U $\lesssim$ 9 m/s), there is a broad overlap among velocity estimates. However, using only the undular hydraulic jump measurements and an assumption of $Fr = 1$ to calculate velocity produces a trend along $d \sim U^2$ in contrast to $d \sim U^{1/2}$ from Jeffreys' equation, which could produce divergent values at the boundaries of undular hydraulic jump stability (low velocity and very high velocity), including at locations very proximal and distal to the vent.

6. Discussion

Re-analysis of comprehensive experiments of undular hydraulic jumps in water and analyses of wave trains in the 2018 Kīlauea lava flow provide compelling evidence that observed wave trains in lava are undular hydraulic jumps. That conclusion allows us to return to questions raised in the introduction about the extent to which hydraulic theory can be used to extract information from wave trains in lava flows, particularly for rapid implementation of flow forecasting models. Importantly, because undular hydraulic jumps represent a transition from supercritical to subcritical flow, physical information derived from wavelength measurements are most accurate where flow is near-critical, which in lava flows often requires good observations close to eruptive vents. Below we briefly review what we have learned about undular hydraulic jumps in water and lava flows, followed by suggestions regarding the optimal lava flow conditions for assessing lava effusion rates in real time. We end with an overview of volcanic settings that may provide opportunities to apply this analysis.

6.1. New Insight Into the Behavior of Undular Hydraulic Jumps in Water Flows

A re-analysis of undular hydraulic jump data from Chanson (1995) reinforces prior analyses (Chanson, 2009; Chanson & Montes, 1995) that show that these waves form as flows transition from supercritical to subcritical states, but only where the initial flow is slightly above critical ($1 \leq Fr \lesssim 2$). In experimental water flows this transition is rapid and flows converge to near-critical flow over an extended reach. Importantly, transitional oscillations can occur in a channel having a fixed smooth bed without any obstructions or abrupt change in bed elevation, bed slope, or flow width (Chanson, 1995). Unlike stationary or isolated hydraulic jumps, which represent an abrupt transition between super- and sub-critical flow where flow energy is expended through a sharp discontinuity involving extreme turbulence and horizontal flow recirculation, undular hydraulic jumps extend this transition longitudinally over multiple waves that oscillate around the critical point. Flow energy in undular hydraulic jumps is dissipated by flow resistance along the bed and sidewalls, as well as turbulence associated with breaking waves (Henderson, 1966).

It may seem surprising that Kennedy's (1960, 1963) theory, which was specifically developed for mobile bed channels, is also applicable to fixed bed channels as well. We speculate that the reason why the theory can be extended to fixed beds at critical flow is because his analytical framework relies on the hypothesis of energy minimization, a condition that is uniquely achieved at critical flow (Henderson, 1966). The implication is that under conditions where undular hydraulic jumps in fixed bed channels are at or near critical flow, Kennedy's (1963) relation should apply.

More generally, undular hydraulic jumps represent a physically defined "brake" for water flows organized by the threshold between supercritical and subcritical flow. Although individual hydraulic jumps may do this locally, undular hydraulic jumps are a mechanism by which supercritical flows converge to near-critical flow. This convergence is generally sustained over several wavelengths before further energy dissipation reduces the flow to subcritical. Within the wave trains themselves, flows oscillate between supercritical and subcritical flow (super- in the troughs, sub- in the crests), somewhat in the manner of a pendulum (Huang et al., 2004). This detailed behavior of wave trains has not, to our knowledge, been reported previously. Importantly, the analyses presented here offer a direct means of estimating mean velocity and flow depth from wavelength, which in turn can be used to calculate flow discharge remotely from scaled imagery if undular hydraulic jumps can be discerned and wavelengths measured. Tinkler (1997) proposed a similar idea for flow in bedrock-channel rivers; our work extends this concept and identifies where and how measurements should be made to conform with theory and experimental observations. It also raises the possibility that similar measurements and interpretations can be made in other high-velocity fluids where wave trains have been reported, such as lahars, hyperconcentrated floods and debris flows (e.g., Pierson & Scott, 1985; Rodolfo et al., 1996).

6.2. Application of Hydraulic Theory to Lava Flows in Near-Real-Time

Despite the different characteristics of water and lava, the universal, rapid convergence of supercritical flow toward critical flow conditions allows application of open-channel hydraulic theory to lava flows. Optimal input data for undular hydraulic jump analysis include both video (for analysis of flow-surface velocities and channel characteristics) and syn-eruptive lidar (for snapshot measurements of undular hydraulic jump wavelength and assessment of post-eruptive channel depth). At a minimum, measurements of channel width and undular hydraulic jump wavelength from calibrated still photographs provide data sufficient to assess mean velocity, depth and effusion rate. Importantly, using undular hydraulic jumps to obtain VER does not require prior knowledge of either the flow slope or the lava viscosity, as required for use of Jeffreys' method (Equation 6).

Our analysis suggests that lava flows produce undular hydraulic jumps only at or near critical flow conditions (Figure 9), a more limited range of Fr than for water flows. This allows us to use Equation 2 to relate measured undular hydraulic jump wavelengths to average flow velocity and, by assuming $Fr = 1$, to flow depth (Equation 3, Figure 10). Near-critical flow of lava requires high flow velocity which, in turn, requires some combination of relatively low viscosity, high effusion rate and/or steep slopes. Importantly, our demonstration that undular hydraulic jumps can form in straight channel reaches if the flow is near-critical, without external forcing (change in slope, bed elevation, or channel width), contrasts with the observation of Le Moigne et al. (2020) that standing waves in lava flows form only at channel disruptions.

When corrected with vesicularity measurements to DRE (Patrick et al., 2019), effusion rates determined from undular hydraulic jumps measured in lidar and UAS imagery obtained within 300 m of the vent are consistent with (a) previous UAS velocimetry analysis and time-averaged discharge rates from time series topographic mapping (Figure 13c; Dietterich et al., 2021), (b) other effusion rate proxies, such as SO_2 emissions (Kern et al., 2020) and (c) those measured from ground-based video and time-lapse imagery (Patrick et al., 2019). Our undular hydraulic jump measurements utilize the best-defined waves (highest amplitudes, strong contrast in crust coverage to identify troughs and crests from incandescence; Figures 8 and 9) and capture the VER from the vent before volume is lost to overflows as it travels down-flow. When flow in the proximal reach is supercritical, measurement locations are shifted downflow to where $Fr \sim 1$. The proximal channel also experiences high and rapidly changing bubble content that will affect bulk effusion rate measurements (Lipman & Banks, 1987; Patrick et al., 2019; Riker et al., 2009). Importantly, our data do not capture any apparent impact of crust growth, degassing, or crystallization on the undular hydraulic jump results.

While undular hydraulic jumps are typically restricted to near-vent (high effusion rate) channel reaches, individual standing waves (stationary hydraulic jumps) have been observed farther from eruptive vents at breaks in slope (e.g., Finch & Macdonald, 1953; Geist et al., 2008; Kauahikaua et al., 1998) and could provide information on flow velocity and depth along lava channels (Le Moigne et al., 2020). Application of hydraulic theory to these features, however, requires caution. In water flows, stationary and undular hydraulic jumps represent two different mechanisms by which energy is extracted from flows. For example, treatment of individual waves as stationary hydraulic jumps (Le Moigne et al., 2020) yields erroneous depths when applied to the undular hydraulic jumps observed in Chanson's (1995) flume experiments (Text S5 and Figure S1 in Supporting Information S1). We suggest, therefore, that the approach proposed by Le Moigne et al. (2020) be applied only to solitary hydraulic jumps.

Is it possible to apply open-channel hydraulic analysis to lava flow features preserved in solidified flows? Neither undular nor stationary hydraulic jumps are preserved in lava channels after flow has ceased. Superelevations produced by lava flowing down a curved channel are preserved and Le Moigne et al. (2020) suggest that hydraulic analysis can also be applied to these features. Superelevation is not, however, the same as a hydraulic jump; rather, it is the manifestation of lava runup that occurs at channel bends. Superelevation does not require critical flow conditions but instead represents a simple conversion of kinetic energy to potential energy through a curve; for this reason, superelevations have been used to estimate flow velocities in lava channels (Guest et al., 1995; Heslop et al., 1989; Kauahikaua et al., 2002; Soule et al., 2004). Flume observations of muddy debris flows, however, caution that simple interpretation of superelevation ignores the possible effects of longitudinal interactions of flow momentum in extending and compressing flows and can therefore overestimate flow velocities (Iverson et al., 2016).

6.3. Applications of Undular Hydraulic Jump Analysis Beyond Active Lava Flows in Hawai‘i

Undular hydraulic jumps are not unique to Hawaiian lava flows. The recent eruption of Fagradalsfjall volcano in Iceland has provided spectacular footage of undular hydraulic jumps (e.g., https://www.youtube.com/watch?v=a1bj6OpJrE4). Similarly, undular hydraulic jumps >5 m amplitude are reported for lava flowing at ~15 m/s during the 2005 eruption of Sierra Negra volcano, Galapagos, Ecuador (volumetric eruption rates ~100 m^3/s; Geist et al., 2008; https://www.youtube.com/watch?v=W72foSDHjJg). Low viscosity (<100 Pa s) lava flows of Cumbre Vieja, La Palma, Spain (Castro & Feisel, 2022), and Nyiragongo volcano, Democratic Republic of the Congo (Giordano et al., 2007), have near-vent velocities >5 m/s and produce thin (<~1 m) flows that are certainly supercritical during emplacement, although proximal observations are limited and published still and video images from these eruptions (Castro & Feisel, 2022; Tazieff, 1977; Tedesco et al., 2007) lack the spatial scales necessary for our application of Equations 2 and 3, retrospectively. However, in these and future eruptions, real-time estimates of lava effusion rates using hydraulic theory would allow rapid assessment of flow parameters for input into hazard models and forecasts of flow advance toward populated areas, such as the large and vulnerable city of Goma downslope of Nyiragongo (Chirico et al., 2009; Tazieff, 1977). To generalize, volcanoes that produce effusive eruption of low viscosity lava at high effusion rates can produce undular hydraulic jumps and are therefore potential targets for the analysis presented here. Such volcanoes are typically located in either divergent boundary or intraplate locations where magma erupts at near-liquidus conditions and low initial H_2O contents limits ascent driven (decompression) crystallization.

7. Concluding Statements

Water and lava differ markedly in their fluid properties but display a remarkable congruence in terms of certain flow dynamics, notably the presence of standing waves. These waves form both as solitary waves and as trains of undular hydraulic jumps. This congruence of fluid dynamic behavior is fundamentally driven by the presence of a physical, energetically determined threshold at critical flow, which separates the subcritical and supercritical flow regimes. Our re-analysis of undular hydraulic jumps in water-flow experiments by Chanson (1995) and analyses of macroscopic flow characteristics of the 2018 Kīlauea lava flow demonstrate a universal tendency toward rapid convergence to critical flow in high-velocity supercritical flow. That universal, rapid convergence is manifest in development of undular hydraulic jumps. Both undular and individual hydraulic jumps represent distinctive standing wave patterns where this convergence threshold occurs—abruptly for individual hydraulic jumps but extending downstream for undular hydraulic jumps. The universal tendency toward critical flow allows us to exploit the macroscopic properties of undular hydraulic jumps to estimate fundamental flow properties of both water and lava. In particular, the rapid convergence to critical flow within the first few waves along undular hydraulic jump wave trains in water allows the wavelengths to be used to estimate mean velocity and flow depth. Our observations of lava channels suggest that critical flow conditions may be maintained for hundreds of meters and multiple waves, thus providing ample opportunity for measurement and analysis.

Volumetric flow rates of channelized flows, such as river discharge and lava effusion rate, are key measurements for assessing hazards and investigating the dynamics of these geophysical flows. Through a multi-fluid analysis of controlled water experiments and unprecedented natural lava flow observations, we demonstrate the application of open channel hydraulic theory across scales and fluid properties. The result is a powerful tool for remotely sensing channelized flow parameters, a tool that can be applied in near-real-time to flows of interest, regardless of accessibility.

More detailed understanding of the dynamics of lava flows at high Froude numbers seems warranted. Data for lava flows are limited by noise and the lack of direct measurements, so future experimental investigations of waves and wave trains in supercritical viscous and multiphase flows would contribute valuable insights that further our understanding of the hydraulics of non-clear-water flows, such as lava and debris flows. The amplitudes of waves across a range of viscosities may also contain hydraulic information that can be usefully exploited. Additionally, close observation of lava effusion from the fissure 8 vent (Ahu‘ailā‘au) at Kīlauea shows that both effusion rates and the physical properties of the lava (especially bubble content) vary on short timescales. Both the bubble content and the effusion rate can affect the rheology of the lava, the latter via a balance among flow advection, cooling, and surface solidification (Griffiths et al., 2003). More importantly, rapidly changing effusion rates raise important challenges to determining an appropriate “mean” effusion rate for use in lava flow models.

Data Availability Statement

All UAS data are available from Desmither et al. (2021) and all lidar data are available from OpenTopography (see USGS, 2018a, 2018b) and Mosbrucker et al. (2020).

Acknowledgments
The authors are deeply indebted to Dr. Hubert Chanson who generously shared his data and provided cogent insights regarding his experiments. This manuscript benefited from comments from Amy East, Christophe Ancey, Roger Denlinger, and three anonymous reviewers. The authors thank the USGS-DOI UAS Kīlauea Response Team, USGS Hawaiian Volcano Observatory, Hawai‘i County Civil Defense, University of Hawai‘i at Hilo, the Federal Emergency Management Agency, and other partners who supported UAS, ground-based video, and lidar data collection during the 2018 Kīlauea eruption response. Supporting Information videos provided by Matt Patrick. Any use of trade, firm, or product names is for descriptive purposes only and does not imply endorsement by the U.S. Government.

References

Amarouchene, Y., & Kellay, H. (2006). Speed of sound from shock fronts in granular flows. *Physics of Fluids*, *18*(3), 031707. https://doi.org/10.1063/1.2185689

Bird, R. B., Stewart, W. E., & Lightfoot, E. N. (2007). *Transport phenomena* (Revised 2nd ed.). Wiley & Sons.

Birnbaum, J., Lev, E., & Llewellin, E. W. (2021). Rheology of three-phase suspensions determined via dam-break experiments. *Proceedings of the Royal Society A*, *477*(2254), 20210394. https://doi.org/10.1098/rspa.2021.0394

Boudet, J. F., Amarouchene, Y., Bonnier, B., & Kellay, H. (2007). The granular jump. *Journal of Fluid Mechanics*, *572*, 413–431. https://doi.org/10.1017/S002211200600365X

Calvari, S., Neri, M., & Pinkerton, H. (2003). Effusion rate estimations during the 1999 summit eruption on Mount Etna, and growth of two distinct lava flow fields. *Journal of Volcanology and Geothermal Research*, *119*(1), 107–123. https://doi.org/10.1016/S0377-0273(02)00308-6

Carn, S. A. (2016). On the detection and monitoring of effusive eruptions using satellite SO_2 measurements. *Geological Society of London Special Publications*, *426*(1), 277–292. https://doi.org/10.1144/sp426.28

Cashman, K. V., Grant, G. G., Dietterich, H. R., & Major, J. J. (2018). Implications of critical flow phenomena for estimating lava flux during recent activity at Kīlauea Volcano. In *American Geophysical Union Fall Meeting Abstracts, 13 December, Washington, DC*.

Cashman, K. V., Kerr, R. C., & Griffiths, R. W. (2006). A laboratory model of surface crust formation and disruption on lava flows through non-uniform channels. *Bulletin of Volcanology*, *68*(7–8), 753–770. https://doi.org/10.1007/s00445-005-0048-z

Cashman, K. V., & Mangan, M. T. (2014). A century of studies of effusive eruptions in Hawai'i. In *US Geological Survey Professional Paper 1801* (pp. 357–394). https://doi.org/10.3133/pp18019

Castro, J. M., & Feisel, Y. (2022). Eruption of ultralow-viscosity basanite magma at Cumbre Vieja, La Palma, Canary Islands. *Nature Communications*, *13*(1), 1–12. https://doi.org/10.1038/s41467-022-30905-4

Castro-Orgaz, O., & Chanson, H. (2022). Free surface profiles of near-critical instabilities in open channel flows: Undular hydraulic jumps. *Environmental Fluid Mechanics*, *22*(2), 275–300. https://doi.org/10.1007/s10652-021-09797-3

Chanson, H. (1995). *Flow characteristics of undular hydraulic jumps: Comparison with near critical flows* (Report CH45/95). Department of Civil Engineering, University of Queensland.

Chanson, H. (2009). Current knowledge in hydraulic jumps and related phenomena. A survey of experimental results. *European Journal of Mechanics – B: Fluids*, *28*(2), 191–210. https://doi.org/10.1016/j.euromechflu.2008.06.004

Chanson, H., & Montes, J. S. (1995). Characteristics of undular hydraulic jumps: Experimental apparatus and flow patterns. *Journal of Hydraulic Engineering*, *121*(2), 129–144. https://doi.org/10.1061/(ASCE)0733-9429(1995)121:2(129)

Chirico, G. D., Favalli, M., Papale, P., Boschi, E., Pareschi, M. T., & Mamou-Mani, A. (2009). Lava flow hazard at Nyiragongo Volcano, DRC. *Bulletin of Volcanology*, *71*(4), 375–387. https://doi.org/10.1007/s00445-008-0232-z

Coppola, D., Laiolo, M., Cigolini, C., Donne, D. D., & Ripepe, M. (2016). Enhanced volcanic hot-spot detection using MODIS IR data: Results from the MIROVA system. *Geological Society of London Special Publications*, *426*(1), 181–205. https://doi.org/10.1144/sp426.5

Costa, A., & Macedonio, G. (2005). Numerical simulation of lava flows based on depth-averaged equations. *Geophysical Research Letters*, *32*(5), L05304. https://doi.org/10.1029/2004GL021817

Cronin, S. J., Neall, V. E., Lecointre, J. A., & Palmer, A. S. (1999). Dynamic interactions between lahars and stream flow: A case study from Ruapehu volcano, New Zealand. *The Geological Society of America Bulletin*, *111*(1), 28–38. https://doi.org/10.1130/0016-7606(1999)111<0028:DIBLAS>2.3.CO;2

Desmither, L. G., Diefenbach, A. K., & Dietterich, H. R. (2021). *Unoccupied Aircraft Systems (UAS) video of the 2018 lower East Rift Zone eruption of Kīlauea Volcano*. U.S. Geological Survey data release. https://doi.org/10.5066/P9BVENTG

Dietterich, H. R., & Cashman, K. V. (2014). Channel networks within lava flows: Formation, evolution, and implications for flow behavior. *Journal of Geophysical Research: Earth Surface*, *119*(8), 1704–1724. https://doi.org/10.1002/2014JF003103

Dietterich, H. R., Diefenbach, A. K., Soule, S. A., Zoeller, M. H., Patrick, M. P., Major, J. J., & Lundgren, P. R. (2021). Lava effusion rate evolution and erupted volume during the 2018 Kīlauea lower East Rift Zone eruption. *Bulletin of Volcanology*, *83*(4), 25. https://doi.org/10.1007/s00445-021-01443-6

Dietterich, H. R., Downs, D. T., Stelten, M. E., & Zahran, H. (2018). Reconstructing lava flow emplacement histories with rheological and morphological analyses: The Harrat Rahat volcanic field, Kingdom of Saudi Arabia. *Bulletin of Volcanology*, *80*(12), 85. https://doi.org/10.1007/s00445-018-1259-4

Eglit, M., Yakubenko, A., & Zayko, J. (2020). A review of Russian snow avalanche models – From analytical solutions to novel 3D models. *Geosciences*, *10*(2), 77. https://doi.org/10.3390/geosciences10020077

Fawer, C. (1937). *Etude de quelques ecoulements permanents á filets courbes* [Study of some steady flows with curved streamlines] (Master thesis; in french). Imprimerie La Concorde.

Finch, R. H., & Macdonald, G. A. (1953). Hawaiian volcanoes during 1950. *US Geological Survey Bulletin*, *996-B*, 49–82. https://doi.org/10.3133/b996B

Gansecki, C., Lee, R. L., Shea, T., Lundblad, S. P., Hon, K., & Parcheta, C. (2019). The tangled tale of Kīlauea's 2018 eruption as told by geochemical monitoring. *Science*, *366*(6470), eaaz0147. https://doi.org/10.1126/science.aaz0147

Garel, F., Kaminski, E., Tait, S., & Limare, A. (2016). A fluid dynamics perspective on the interpretation of the surface thermal signal of lava flows. *The Geological Society of London, Special Publications*, *426*(1), 243–256. https://doi.org/10.1144/SP426.6

Geist, D. J., Harpp, K. S., Naumann, T. R., Poland, M., Chadwick, W. W., Hall, M., & Rader, E. (2008). The 2005 eruption of Sierra Negra volcano, Galápagos, Ecuador. *Bulletin of Volcanology*, *70*(6), 655–673. https://doi.org/10.1007/s00445-007-0160-3

Gilbert, G. K. (1914). *The transportation of debris by running water* (Professional Paper 86). US Geological Survey.

Giordano, D., Polacci, M., Longo, A., Papale, P., Dingwell, D. B., Boschi, E., & Kasereka, M. (2007). Thermo-rheological magma control on the impact of highly fluid lava flows at Mt. Nyiragongo. *Geophysical Research Letters*, *34*(6), L06301. https://doi.org/10.1029/2006GL028459

Grant, G. E. (1997). Critical flow constrains flow hydraulics in mobile-bed streams: A new hypothesis. *Water Resources Research*, *33*(2), 349–358. https://doi.org/10.1029/96WR03134

Gray, J. M. N. T., Tai, Y. C., & Noelle, S. (2003). Shock waves, dead zones and particle-free regions in rapid granular free-surface flows. *Journal of Fluid Mechanics*, *491*, 161–181. https://doi.org/10.1017/S0022112003005317

Griffiths, R. W. (2000). The dynamics of lava flows. *Annual Review of Fluid Mechanics*, *32*(1), 477–518. https://doi.org/10.1146/annurev.fluid.32.1.477

Griffiths, R. W., Kerr, R. C., & Cashman, K. V. (2003). Patterns of solidification in channel flows with surface cooling. *Journal of Fluid Mechanics*, *496*, 33–62. https://doi.org/10.1017/S0022112003006517

Grigorian, S. S., & Ostroumov, A. V. (2020). On a continuum model for avalanche flow and its simplified variants. *Geosciences*, *10*(1), 35. https://doi.org/10.3390/geosciences10010035

Gudmundsson, M. T. (2015). Hazards from lahars and jökulhlaups. In H. Sigurdsson, B. Houghton, S. McNutt, H. Rymer, & J. Stix (Eds.), *The encyclopedia of volcanoes* (pp. 971–984). Academic Press. https://doi.org/10.1016/B978-0-12-385938-9.00056-0

Guest, J. E., Spudis, P. D., Greeley, R., Taylor, G. J., & Baloga, S. M. (1995). Emplacement of xenolith nodules in the Kaupulehu lava flow, Hualalai Volcano, Hawaii. *Bulletin of Volcanology*, *57*(3), 179–184. https://doi.org/10.1007/BF00265037

Hákonardóttir, K. M., & Hogg, A. J. (2005). Oblique shocks in rapid granular flows. *Physics of Fluids*, *17*(7), 077101. https://doi.org/10.1063/1.1950688

Harris, A. J. L., & Baloga, S. M. (2009). Lava discharge rates from satellite-measured heat flux. *Geophysical Research Letters*, *36*(19), L19302. https://doi.org/10.1029/2009GL039717

Harris, A. J. L., De Groeve, T., Carn, S. A., & Garel, F. (2016). Risk evaluation, detection and simulation during effusive eruption disasters. *The Geological Society of London, Special Publications*, *426*, 1–22. https://doi.org/10.1144/SP426.29

Harris, A. J. L., Dehn, J., & Calvari, S. (2007). Lava effusion rate definition and measurement: A review. *Bulletin of Volcanology*, *70*(1), 1–22. https://doi.org/10.1007/s00445-007-0120-y

Harris, A. J. L., Villeneuve, N., Di Muro, A., Ferrazzini, V., Peltier, A., Coppola, D., et al. (2017). Effusive crises at Piton de la Fournaise 2014–2015: A review of a multi-national response model. *Journal of Applied Volcanology*, *6*(1), 11. https://doi.org/10.1186/s13617-017-0062-9

Henderson, F. M. (1966). *Open channel flow*. The Macmillan Co.

Heslop, S. E., Wilson, L., Pinkerton, H., & Head, J. W. (1989). Dynamics of a confined lava flow on Kilauea volcano, Hawaii. *Bulletin of Volcanology*, *51*(6), 415–432. https://doi.org/10.1007/BF01078809

Huang, H. Q., Chang, H. H., & Nanson, G. C. (2004). Minimum energy as the general form of critical flow and maximum flow efficiency and for explaining variations in river channel pattern. *Water Resources Research*, *40*(4), W04502. https://doi.org/10.1029/2003WR002539

Iverson, R. M., & Denlinger, R. P. (2001). Flow of variably fluidized granular masses across three-dimensional terrain: 1. Coulomb mixture theory. *Journal of Geophysical Research*, *106*(B1), 537–552. https://doi.org/10.1029/2000JB900329

Iverson, R. M., George, D. L., & Logan, M. (2016). Debris flow runup on vertical barriers and adverse slopes. *Journal of Geophysical Research: Earth Surface*, *121*(12), 2333–2357. https://doi.org/10.1002/2016JF003933

Jeffreys, H. (1925). The flow of water in an inclined channel of rectangular section. *The London, Edinburgh, and Dublin Philosophical Magazine and Journal of Science*, *49*(293), 793–807. https://doi.org/10.1080/14786442508634662

Kauahikaua, J., Cashman, K. V., Clague, D., Champion, D., & Hagstrum, J. (2002). Emplacement of the most recent lava flows on Hualālai Volcano, Hawai'i. *Bulletin of Volcanology*, *64*(3), 229–253. https://doi.org/10.1007/s00445-001-0196-8

Kauahikaua, J., Cashman, K. V., Mattox, T. N., Heliker, C., Hon, K. A., Mangan, M. T., & Thornber, C. R. (1998). Observations on basaltic lava streams in tubes from Kilauea Volcano, island of Hawai'i. *Journal of Geophysical Research*, *103*(B11), 27303–27323. https://doi.org/10.1029/97JB03576

Kauahikaua, J., Sherrod, D. R., Cashman, K. V., Heliker, C., Hon, K., Mattox, T. N., & Johnson, J. A. (2003). Hawaiian lava-flow dynamics during the Puu Oo-Kupaianaha eruption: A tale of two decades. In C. C. Heliker, D. A. Swanson, & T. J. Takahashi (Eds.), *The Pu'u 'Ō'ō-Kūpaianaha Eruption of Kīlauea Volcano, Hawai'i: The first 20 years* (Professional Paper 1676, pp. 63–87). US Geological Survey.

Kennedy, J. F. (1960). *Stationary waves and antidunes in alluvial channels* (PhD thesis). California Institute of Technology.

Kennedy, J. F. (1961). *Stationary waves and antidunes in alluvial channels* (Report KH-R-2). W. M. Keck Laboratory of Hydraulics and Water Resources, California Institute of Technology.

Kennedy, J. F. (1963). The mechanics of dunes and antidunes in erodible-bed channels. *Journal of Fluid Mechanics*, *16*(4), 521–544. https://doi.org/10.1017/S0022112063000975

Kern, C., Lerner, A. H., Elias, T., Nadeau, P. A., Holland, L., Kelly, P. J., et al. (2020). Quantifying gas emissions associated with the 2018 rift eruption of Kīlauea Volcano using ground-based DOAS measurements. *Bulletin of Volcanology*, *82*(7), 55. https://doi.org/10.1007/s00445-020-01390-8

Kieffer, S. W. (1985). The 1983 hydraulic jump in Crystal rapid: Implications for river-running and geomorphic evolution in the Grand Canyon. *The Journal of Geology*, *93*(4), 385–406. https://doi.org/10.1086/628962

Le Moigne, Y., Zurek, J. M., Williams-Jones, G., Lev, E., Calahorrano-Di Patre, A., & Anzieta, J. (2020). Standing waves in high speed lava channels: A tool for constraining lava dynamics and eruptive parameters. *Journal of Volcanology and Geothermal Research*, *401*, 106944. https://doi.org/10.1016/j.jvolgeores.2020.106944

Lev, E., & James, M. R. (2014). The influence of cross-sectional channel geometry on rheology and flux estimates for active lava flows. *Bulletin of Volcanology*, *76*(7), 829. https://doi.org/10.1007/s00445-014-0829-3

Lev, E., Spiegelman, M., Wysocki, R. J., & Karson, J. A. (2012). Investigating lava flow rheology using video analysis and numerical flow models. *Journal of Volcanology and Geothermal Research*, *247*(248), 62–73. https://doi.org/10.1016/j.jvolgeores.2012.08.002

Lipman, P. W., & Banks, N. G. (1987). Aa flow dynamics, Mauna Loa 1984. In R. W. Decker, T. L. Wright, & P. H. Stauffer (Eds.), *Volcanism in Hawaii* (Professional Paper 1350, pp. 1527–1567). US Geological Survey.

Llewellin, E. W., & Manga, M. (2005). Bubble suspension rheology and implications for conduit flow. *Journal of Volcanology and Geothermal Research*, *143*(1), 205–217. https://doi.org/10.1016/j.jvolgeores.2004.09.018

Lyons, J. J., Dietterich, H. R., Patrick, M. P., & Fee, D. (2021). High-speed lava flow infrasound from Kīlauea's fissure 8 and its utility in monitoring effusion rate. *Bulletin of Volcanology*, *83*(11), 66. https://doi.org/10.1007/s00445-021-01488-7

Macdonald, G. A. (1943). The 1942 eruption of Mauna Loa, Hawai'i. *American Journal of Science*, *241*(4), 241–256. https://doi.org/10.2475/ajs.241.4.241

Mader, H. M., Llewellin, E. W., & Mueller, S. P. (2013). The rheology of two-phase magmas: A review and analysis. *Journal of Volcanology and Geothermal Research*, *257*, 135–158. https://doi.org/10.1016/j.jvolgeores.2013.02.014

Montes, J. S., & Chanson, H. (1998). Characteristics of undular hydraulic jumps: Experiments and analysis. *Journal of Hydraulic Engineering*, *124*(2), 192–205. https://doi.org/10.1061/(ASCE)0733-9429(1995)121:2(129)

Mosbrucker, A. R., Zoeller, M. H., & Ramsey, D. W. (2020). *Digital elevation model of Kīlauea Volcano, Hawaii, based on July 2019 airborne lidar surveys*. US Geological Survey Data Release. https://doi.org/10.5066/P9F1ZU8O

Murphy, E. C. (1910). The behavior of a stream carrying sand and the effect of sand on the measurement of bottom velocity. *Engineering News*, *63*(20), 580–581.

Neal, C. A., Brantley, S. R., Antolik, L., Babb, J. L., Burgess, M., Calles, K., et al. (2019). The 2018 rift eruption and summit collapse of Kīlauea Volcano. *Science*, *363*(6425), 367–374. https://doi.org/10.1126/science.aav7046

Ohtsu, I., Yasuda, Y., & Gotoh, H. (2001). Hydraulic condition for undular-jump formations. *Journal of Hydraulic Research*, *39*(2), 203–209. https://doi.org/10.1080/00221680109499821

Ohtsu, I., Yasuda, Y., & Gotoh, H. (2003). Flow Conditions of undular hydraulic jumps in horizontal rectangular Channels. *Journal of Hydraulic Engineering*, *129*(12), 948–955. https://doi.org/10.1061/(ASCE)0733-9429

Patrick, M. R., Dietterich, H. R., Lyons, J. J., Diefenbach, A. K., Parcheta, C., Anderson, K. R., et al. (2019). Cyclic lava effusion during the 2018 eruption of Kīlauea Volcano. *Science*, *366*(6470), eaay9070. https://doi.org/10.1126/science.aay9070

Pierson, T. C. (1985). Initiation and flow behavior of the 1980 Pine Creek and muddy river lahars, Mount St. Helens, Washington. *GSA Bulletin*, *96*(8), 1056–1069. https://doi.org/10.1130/0016-7606(1985)96<1056:IAFBOT>2.0.CO;2

Pierson, T. C., & Scott, K. M. (1985). Downstream dilution of a lahar: Transition from debris flow to hyperconcentrated streamflow. *Water Resources Research*, *21*(10), 1511–1524. https://doi.org/10.1029/WR021i010p01511

Pinkerton, H., & Wilson, L. (1994). Factors controlling the lengths of channel-fed lava flows. *Bulletin of Volcanology*, *56*(2), 108–120. https://doi.org/10.1007/BF00304106

Piton, G., & Recking, A. (2019). Steep bedload-laden flows: Near critical? *Journal of Geophysical Research: Earth Surface*, *124*(8), 2160–2175. https://doi.org/10.1029/2019JF005021

Pringle, P. T., & Cameron, K. A. (1999). Eruption-triggered lahar on May 14, 1984. In T. C. Pierson (Ed.), *Hydrologic consequences of hot-rock/snowpack interactions at Mount St. Helens Volcano, Washington, 1982–84* (Professional Paper 1586, pp. 81–103). US Geological Survey.

Rhéty, M., Harris, A., Villeneuve, N., Gurioli, L., Médard, E., Chevrel, O., & Bachélery, P. (2017). A comparison of cooling-limited and volume-limited flow systems: Examples from channels in the Piton de la Fournaise April 2007 lava-flow field. *Geochemistry, Geophysics, Geosystems*, *18*(9), 3270–3291. https://doi.org/10.1002/2017GC006839

Richter, D. H., Eaton, J. P., Murata, K. J., Ault, W. U., & Krivoy, H. L. (1970). *Chronological narrative of the 1959–60 eruption of Kilauea Volcano, Hawaii* (Professional Paper 537E). US Geological Survey. https://doi.org/10.3133/pp537E

Riker, J. M., Cashman, K. V., Kauahikaua, J. P., & Montierth, C. M. (2009). The length of channelized lava flows: Insight from the 1859 eruption of Mauna Loa Volcano, Hawai'i. *Journal of Volcanology and Geothermal Research*, *183*(3–4), 139–156. https://doi.org/10.1016/j.jvolgeores.2009.03.002

Rodolfo, K. S., Umbal, J. V., Alonso, R. A., Remotigue, C. T., Paladio-Melosantos, M. L., Salvador, J. H. G., et al. (1996). Two years of lahars on the western flank of Mount Pinatubo: Initiation, flow processes, deposits, and attendant geomorphic and hydraulic changes. In C. G. Newhall & R. S. Punungbayan (Eds.), *Fire and mud: Eruptions and lahars of Mount Pinatubo, Philippines* (pp. 989–1013). University of Washington Press.

Rowland, S. K., & Walker, G. P. L. (1990). Pahoehoe and aa in Hawaii: Volumetric flow rate controls the lava structure. *Bulletin of Volcanology*, *52*(8), 615–628. https://doi.org/10.1007/BF00301212

Rust, A. C., & Manga, M. (2002). Effects of bubble deformation on the viscosity of dilute suspensions. *Journal of Non-Newtonian Fluid Mechanics*, *104*(1), 53–63. https://doi.org/10.1016/S0377-0257(02)00013-7

Sano, M., & Tamai, K. (2016). A universal transition to turbulence in channel flow. *Nature Physics*, *12*(3), 249–253. https://doi.org/10.1038/nphys365

Soule, S. A., Cashman, K. V., & Kauahikaua, J. P. (2004). Examining flow emplacement through the surface morphology of three rapidly emplaced, solidified lava flows, Kīlauea Volcano, Hawai'i. *Bulletin of Volcanology*, *66*, 1–14. https://doi.org/10.1007/s00445-003-0291-0

Takagi, D., & Huppert, H. E. (2010). Initial advance of long lava flows in open channels. *Journal of Volcanology and Geothermal Research*, *195*(2), 121–126. https://doi.org/10.1016/j.jvolgeores.2010.06.011

Tallarico, A., & Dragoni, M. (1999). Viscous Newtonian laminar flow in a rectangular channel: Application to Etna lava flows. *Bulletin of Volcanology*, *61*(1), 40–47. https://doi.org/10.1007/s004450050261

Tazieff, H. (1977). An exceptional eruption: Mt. Niragongo, Jan. 10th, 1977. *Bulletin of Volcanology*, *40*(3), 189–200. https://doi.org/10.1007/BF02596999

Tedesco, D., Vaselli, O., Papale, P., Carn, S. A., Voltaggio, M., Sawyer, G. M., et al. (2007). January 2002 volcano-tectonic eruption of Nyiragongo volcano, Democratic Republic of Congo. *Journal of Geophysical Research*, *112*(B9), B09202. https://doi.org/10.1029/2006JB004762

Thielicke, W., & Stamhuis, E. (2014). PIVlab – Towards user-friendly, affordable and accurate digital particle image velocimetry in MATLAB. *Journal of Open Research Software*, *2*(1), e30. https://doi.org/10.5334/jors.bl

Tinkler, K. J. (1997). Indirect velocity measurement from standing waves in rockbed rivers. *Journal of Hydraulic Engineering*, *123*(10), 918–921. https://doi.org/10.1061/(ASCE)0733-9429(1997)123:10(918)

USGS. (2018a). Kilauea Volcano, HI July 2018 acquisition airborne lidar survey. U.S. Geological Survey in collaboration with the State of Hawaii, Federal Emergency Management Agency, Cold Regions Research and Engineering Laboratory, and the National Center for Airborne Laser Mapping. Distributed by OpenTopography. https://doi.org/10.5069/G9M32SV1

USGS. (2018b). Kilauea Volcano, June HI 2018 Acquisition airborne lidar survey. U.S. Geological Survey in collaboration with GEO1, Windward Aviation, Quantum Spatial, and Cold Regions Research and Engineering Laboratory. Distributed by OpenTopography. https://doi.org/10.5069/G98K7718

Viroulet, S., Baker, J., Edwards, A., Johnson, C., Gjaltema, C., Clavel, P., & Gray, J. (2017). Multiple solutions for granular flow over a smooth two-dimensional bump. *Journal of Fluid Mechanics*, *815*, 77–116. https://doi.org/10.1017/jfm.2017.41

Vreugdenhil, C. B. (1994). *Numerical methods for shallow-water flow* (Vol. 13). Springer Science & Business Media.

Walker, G. P. L., Guest, J. E., & Skelhorn, R. R. (1973). Mount Etna and the 1971 eruption – Lengths of lava flows. *Philosophical Transactions of the Royal Society of London – Series A: Mathematical and Physical Sciences*, *274*(1238), 107–118. https://doi.org/10.1098/rsta.1973.0030

Wolfe, E. W. (1988). *The Puu Oo eruption of Kilauea volcano, Hawaii: Episodes 1 through 20, January 3, 1983, through June 8, 1984* (Professional Paper 1463, p. 251). US Geological Survey. https://pubs.er.usgs.gov/publication/pp1463